UNIVERSITY OF OKLAHOMA

GRADUATE COLLEGE

Tensile Behavior of Ultra-High Performance Concrete Under Direct Tension

A THESIS

SUBMITTED TO THE GRADUATE FACULTY

In partial fulfillment of the requirement for
the degree of

MASTER OF SCIENCE

By

KEVIN J. G. LEPISSIER

Norman, Oklahoma

2020

TENSILE BEHAVIOR OF ULTRA-HIGH PERFORMANCE CONCRETE UNDER DIRECT TENSION

A THESIS APPROVED FOR THE SCHOOL OF CIVIL ENGINEERING AND ENVIRONMENTAL SCIENCE

BY THE COMMITTEE CONSISTING OF

BY

Dr. Jeffery S. Volz, Chair

Dr. Royce W. Floyd

Dr. P. Scott Harvey

Acknowledgements

Contents

List of Tables

List of Figures

Abstract

Ultra-High Performance Concrete (UHPC) is a product that has improved mechanistic properties as compared to traditional concrete and is defined by the Federal Highway Administrations (FHWA) as having a post-cracking tensile strength of 0.72 ksi with a minimum compressive strength of 21.7 ksi. UHPC has constituents that are used to improve the various properties of the concrete. One such constituent is steel fibers, which help to improve the flexural strength of the concrete and the post-cracking strength. There are a variety of different UHPC mix designs, but for this study, the non-proprietary J3 UHPC mix from the University of Oklahoma was used. This study also sought to determine the optimum fiber content in UHPC for strain hardening and to evaluate whether the cylindrical dogbone specimen offers the greatest potential for the Direct Tension Test (DTT).

The cylindrical dogbone was chosen because it has reduced stress concentrations and uniform stress distribution compared to the typical prismatic FHWA specimen. This study examined the effects of different fiber contents (0% to 6%) on the tensile capacity and behavior of UHPC. Upon completion of the testing, it was found that 4% fiber content had the best overall tensile performance for the J3 UHPC mix.

A study was also completed in order to show the stress distribution in three different specimen types – a cylindrical dogbone specimen, a 2 inch x 4 inch cylindrical specimen, and a 2 inch x 2 inch x 17 inch FHWA specimen. All three specimens were tested in direct tension and modelled in ANSYS. The results showed that the cylindrical dogbone specimen had lower stress concentrations as compared to the FHWA specimen and improved bonding with the end anchorages compared to the cylindrical specimen due to the enlarged end regions. The cylindrical dogbone specimen is recommended for tension testing of UHPC.

1 Introduction

1.1 Background and Reasoning

For centuries, conventional concrete has been used to construct much of humanity's structures, both vertically and horizontally, primarily due to its readily available components and relative ease of mixing and placing. This has also led to conventional concrete being well researched and tested. However, due to constant innovation and the need for longer lasting, more durable structures, several new concrete mixtures and materials have been created. Ultra-High Performance Concrete (UHPC) is one such creation. Ductal®, a product from Lafarge has been around for approximately 21 years, and in addition, the Federal Highway Administration (FHWA) states that UHPC has been commercially available since 2000 (FHWA, 2019).

The FHWA defines UHPC as follows:

> *UHPC is a cementitious composite material composed of an optimized gradation of granular constituents, a water-to-cementitious materials ratio less than 0.25, and a high percentage of discontinuous internal fiber reinforcement. In general, the mechanical properties of UHPC include compressive strength greater than 21.7 ksi (150 MPa) and sustained post-cracking tensile strength greater than 0.72 ksi (5 MPa).*

UHPC is a cementatious composite material that has improved mechanistic properties, improved bond strength, and excellent durability and ductility compared to conventional concrete (Savino et al., 2018). One key factor that improves UHPC is through the addition of steel fibers to the mix, which improves the post-cracking tensile strength and behavior (Benjamin and Floret, 2013). Typically, UHPC that has fibers added to it is referred to as Ultra-High Performance Fiber-Reinforced Concrete (UHPFRC), but henceforth UHPC will be used to

replace UHPFRC. In contrast to conventional concrete, UHPC requires less material to achieve higher load transfer and improved behavior.

There are various available mix designs for UHPC, but for this research, the non-proprietary J3 mix design developed at the University of Oklahoma (McDaniel, 2017) was used for all testing. This UHPC mix is composed of silica fume, ground-granulated blast furnace slag (GGBFS), Type 1 cement, steel fibers, masonry sand, water, and a high range water reducer (HRWR). Silica fume and GGBFS are important to UHPC as they typically improve the economy of the mix, the durability of the concrete, and the long-term strength (McDaniel, 2017). The water to cementitious material (w/cm) ratio was set at 0.2. In addition to this HRWR was added to increase the overall workability. Glenium 7920 produced by the BASF Corporation was used as the HRWR. Since UHPC does not have coarse aggregate like conventional concrete, masonry sand was used instead, with properties in accordance with ASTM C33.

It is important to note that the flexural strength of UHPC has been researched far more than its direct tensile strength. Of the two tests to conduct, flexural strength is easier to do. There are two test methods to determine the tensile capacity of concrete: the Direct Tension Test (DTT) and the Indirect Tension Test (ITT). Both of these test methods have their respective advantages and disadvantages, however the DTT is preferred due to its simplicity to correlate the test method to the experimental tension results. One of the first DTT methods was developed in 1928, where a 6 in diameter concrete cylinder was gripped by the ends and pulled apart (Graybeal and Baby, 2013). Two separate DTTs have been developed since 1928: the bonding method and the gripping method. The bonding method involves using adhesives to attach a metal plate to the concrete specimen, which in turn will be pulled apart. The gripping method directly grips the concrete specimen and pulls it apart (Graybeal and Baby, 2013).

1.2 Objectives and Goals

The primary goal of this research study is to evaluate the performance and behavior of UHPC in direct tension. The supporting objectives and secondary goals consist of the following:

1.2.1 Objectives

The objectives of the research study consist of the following:

a. Test various fiber contents in direct tension then evaluate the results to determine the best fiber content

b. Compare stress distributions between different potential UHPC tension testing specimen types (cylindrical dogbone, 2 inch x 4 inch cylinder, and the FHWA prism)

c. Use ANSYS to analyze the stress distributions and potential concentrations within the different specimen types (cylindrical dogbone, 2 inch x 4 inch cylinder, and a FHWA prism)

1.2.2 Goals

The goals of the research study consist of the following:

a. Determine the best fiber content and ultimate tensile strength of UHPC

b. Evaluate whether the cylindrical dogbone specimen offers the best potential for tension testing of UHPC

c. Understand the post-cracking behavior of UHPC with various fiber contents

1.3 Outline

This thesis consists of the following eight chapters:

1. Chapter 1 – Introduction: This chapter presents the background behind this research as well as the main goals and objectives.

2. Chapter 2 – Literature Review: This chapter summarizes the literature relevant to this study.

3. Chapter 3 – Research Program: This chapter briefly describes the reasoning behind this research and provides a brief description into the different tasks that were conducted.

4. Chapter 4 – Cylindrical Dogbone Tension Test: This chapter goes into depth about the methods and results of tension tests of the cylindrical dogbone specimen.

5. Chapter 5 – Stress Distribution Study: This chapter outlines the methodology of the specimen stress distribution testing and provides the accompanying results.

6. Chapter 6 – Analytical Study: This chapter provides a description of the finite element analytical modelling and provides the associated results.

7. Chapter 7 – Analysis of Results: This chapter analyzes the result from the testing and analytical modeling tasks.

8. Chapter 8 – Findings, Conclusions and Recommendations – This is the final chapter before the appendix and summarizes the findings, conclusions, and recommendations of the research study.

2 Literature Review

2.1 Direct Tension Test (DTT) and Dogbone Specimen

While there are many different methods to determine the tensile strength of UHPC, the main test method outlined in ASTM C1583 was used. For the main topic of this research, to test the optimal fiber content for strain hardening, a cylindrical dogbone specimen will be used for the DTT. In addition to this, two 2 inch x 4 inch cylindrical specimens and two 2 inch x 2 inch x 17 inch FHWA prisms will be tested. Graybeal (2011) stated that the tensile testing of UHPC can be done the same way as conventional concrete; however, there is no standardized tension test to determine the post cracking capacity of UHPC. There is a need to find a way to test the tensile capacity post-crack, and that is part of what this research will aim to do.

There are numerous testing procedures to characterize the tensile behavior in UHPC, but DTTs are preferred to indirect tension tests (ITT) such as the splitting tension test (Savino et al., 2018). Savino et al. (2018), looked at the behavior of Steel Fiber Reinforced Concrete and the relationship the DTT has to ITT. Within the research, three fiber types were examined: hooked, straight (0.3mm) and straight (0.175mm). These provided reasonable tensile strengths for the mix; however, it did not show the best fiber content, rather just a generic mix. Savino et al. (2018) also indicated that the DTT used a prismatic dogbone specimen, as it provides the best results for UHPC testing. The tests carried out were extensive and included the three fiber types, the mix type and the number of days cured, as shown in Table 2.1.

Table 2.1 Specimen Identification (Savino et al., 2018)

A, B, C	Type of SFRC
1, 2, 3, 4	Day of Casting
b, ub, d, c	Beam, un-notched beam, dog-bone, cubic specimen
I, II, III	Number of specimens of a given series

The results, shown in Table 2.2, will serve as a good reference point and comparison to this research. It is important to note that specimens denoted with B and C will be the best comparison, as they are both UHPC mixes and have a fiber content of 2.5% and 3.8% respectively.

Table 2.2 Results from Savino et al. (2018)

Dog-Bone Specimen	$F_{t,i}$ (MPa {psi})	Dog-Bone Specimen	$F_{t,i}$ (MPa {psi})
A.1.d-I	6.52 {945.4}	B.2.d-I	14.80 {2146}
A.1.d-II	5.60 {812.0}	B.2.d-II	11.76 {1705}
A.1.d-III	5.79 {839.6}	B.2.d-III	13.73 {1991}
A.2.d-I	7.51 {1089}	C.1.d-I	14.45 {2095}
A.2.d-II	6.77 {981.7}	C.1.d-II	11.76 {1705}
A.2.d-III	6.90 {1001}	C.1.d-III	11.28 {1636}
A.3.d-I	5.42 {785.9}	C.2.d-I	12.43 {1802}
A.3.d-II	5.94 {861.3}	C.2.d-II	11.55 {1675}
A.3.d-III	6.38 {925.1}	C.2.d-III	14.49 {2101}
A.4.d-I	6.15 {891.8}	C.3.d-I	13.85 {2008}
A.4.d-II	5.20 {754}	C.3.d-II	13.80 {2001}
A.4.d-III	7.46 {1082}	C.3.d-III	13.67 {1982}
B.1.d-I	10.31 {1495}	C.4.d-I	13.80 {2001}
B.1.d-II	10.44 {1514}	C.4.d-II	13.58 {1969}
B.1.d-III	10.02 {1453}	C.4.d-III	12.11 {1756}

Wille et al. (2014) performed an analytical and experimental investigation of the uniaxial tensile behavior using the DTT. It is quite difficult to test materials that exhibit strain hardening when accompanied by multiple crack locations, such as with UHPC. This is one of the key factors as to why there is currently no standardized test available (Willle et al., 2014). This study showed a comparison of the DTT that can potentially be used and the shortcomings of each. Figure 2.1 (Wille et al., 2014) shows the different concrete specimens along with its corresponding type of the DTT performed. From this one figure, it is clear to see the variation of

configurations that can be used for the DTT. Wille et al. (2014) largely considered prismatic dogbone specimens, and although this is very typical in practice, there are some drawbacks to using this type. Any prismatic concrete specimen will have large stress concentrations, which cause failures, thus lowering the effective tensile strength that can be captured.

Shape dogbone	Material (–)	Performance level (–)	Length, width and depth of constant area (total specimen) in (mm)			Diff. area	Grip/attachment	DOF[a] top–bottom
			L	W	D			
	UHP-FRC	4	80	30	13	50%	Fixed	0–0
			(330)	(60)	(13)			
	HPFRCC	3–4	80	24	40	60%	Fixed	0–0
			(240)	(40)	(40)			
	HPFRCC	4	152	38	76	50%	Self-clamping friction grip[b]	1–1
			(457)	(76)	(76)			
	HPFRCC	3	150	25	25	63%	Anchored/pinned	1–1
			(200)	(40)	(25)			
	HPFRCC	3	200	50	13	40%	Anchored/pinned	1–1
			(525)	(125)	(13)			
	UHP-FRC	3–4	178	51	25	41%	Anchored/pinned	1–1
			(525)	(125)	(25)			
	UHP-FRC	3–4	200	100	50	33%	Top glued/anchored	0–0
			(750)	(300)	(50)			
	UHP-FRC	3	250	100	35	50%	Side glued/pinned	1–1
			(740)	(200)	(35)			
	UHP-FRC	3	200	160	45	80%	Side glued + anchored (greased)	0–0
			(700)	(200)	(45)			
	HPFRCC	3–4	80	30	13/30	50%	Clamped/fixed/pinned	0/2–0/2
			(330)	(60)	(13/30)			
	Plain concrete	0	200	60	100	60%	Top glued	0–0
			(400)	(100)	(100)			
	Plain concrete	0	0[c]	60[c]	100[c]	60%	Top glued/pinned	2–2
			(150)[c]	(100)[c]	(100)[c]			
	Plain lightweight concrete	0	0	80[d]	–	64%	Top glued/fixed	0–0
			(270)	(100)[d]				
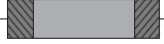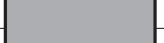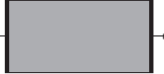
[a] DOF – degree of freedom.
[b] Similar to Saito and Imai [15].
[c] Other sizes were also investigated.
[d] Diameter of the cylinder.

Figure 2.1 Dogbone Specimens (Wille et al., 2014)

7

The prism and cylindrical specimen setup are also evaluated in research conducted by Wille et al. (2014) and are shown in Figure 2.2.

Shape unnotched prism/cylinder	Material (–)	Performance level (–)	Length, width and depth of constant area (total specimen) in (mm)			Diff. area	Grip/attachment	DOF[a]top–bottom
			L	W	D			
	FRC	<3	127	127	28	100%	Side glued/pinned	0–0
			(330)	(127)	(28)			
	FRC/ECC	3/4	205	76	13	100%	Side glued/pinned	0–0
			(305)	(76)	(13)			
	UHP-FRC	3	102	51	51	100%	Side glued + clamped /fixed	0–0
			(432)	(51)	(51)			
	UHP-FRC	3	160	70	70	100%	Top glued	0–0
			(160)	(70)	(70)			
	Plain concrete/UHP-FRC	0/3	200	100[b]	–	100%	op glued	0–0
			(200)	(100)[b]				

[a] DOF – degree of freedom.
[b] Diameter of the cylinder.

Figure 2.2 Prism/Cylinder Unnotched Specimens (Wille et al., 2014)

The performance level that is attached to each specimen is an indication into whether or not it is a good specimen for strain hardening. A performance level of 4 will provide the best results for strain hardening whereas a level of 0 will perform poorly. It is clear from Figure 2.1 that certain dogbone specimens will be adequate for the DTT and for the determination of strain hardening. In order for the dogbone specimen to be accurate, Wille et al. (2014) states that these three conditions need to be met: (a) a large cross-sectional area at the ends for adequate support bonding, (b) a smooth transition between ends and middle section to avoid stress concentrations and (c) a middle section with constant or nearly constant cross-sectional area to promote multiple cracking behavior.
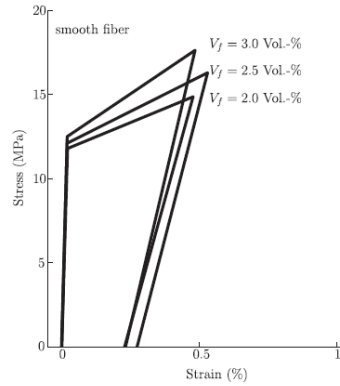
Figure 2.3 Comparison of Bi-linear Models for all Fiber Contents (Wille et al., 2014)

Graybeal and Baby (2013) also conducted research into the tensile strength of UHPC, reiterating the fact that there is no standardized DTT. The "dogbone test" was used in this research, which correlates to that found in Wille et al. (2014), and the results from Graybeal and Baby (2013) can be seen in Table 2.3 and 2.4. Each specimen set has different curing regimes, fiber contents, and length of dogbone. The F1A- long specimen will be the best comparison to the results obtained from this study, however, again a clamping grip method was used instead of the epoxy method that will be performed in this study.

Table 2.3 Results of Grip Test DTT (a) (Graybeal and Baby, 2013)

Specimen set	Elastic modulus (GPa {ksi})	Average first cracking strength (MPa {psi})	Facial first cracking strength (MPa {psi})
F1A-Long	55.8 {8093}	9.09 {1318}	12.83 {1861}
F1A-Short	54.5 {7905}	8.52 {1236}	12.05 {1748}
F2A-Long	56.5 {8195}	6.67 {967}	10.08 {1462}
F2A-Short	55.4 {8035}	5.91 {857}	10.25 {1487}
F1C-Long	54.2 {7861}	9.07 {1315}	10.34 {1500}
F1C-Short	56.1 {8137}	8.41 {1220}	11.09 {1608}
B2A-Short	61.7 {8949}	6.18 {896}	9.29 {1347}

Table 2.4 Results of Grip Test DTT (b) (Graybeal and Baby, 2013)

Specimen set	Average multi-cracking stress, (MPa {psi})	Maximum tensile strength, (MPa {psi})	Strain at saturation	Strain at localization
F1A-Long	9.97 {1446}	11.20 {1624}	0.004170	0.004720
F1A-Short	9.18 {1331}	10.29 {1492}	0.005390	0.005920
F2A-Long	8.47 {1228}	9.18 {1331}	0.00305	0.003410
F2A-Short	7.76 {1125}	8.56 {1242}	0.00390	0.004760
F1C-Long	10.59 {1536}	11.56 {1677}	0.005240	0.005842
F1C-Short	10.49 {1521}	11.36 {1648}	0.004840	0.005685
B2A-Short	9.36 {1358}	10.53 {1527}	0.004230	0.006480

It is important to note that throughout the multiple studies conducted on UHPC and tensile strength, there is no study for the optimum fiber content that exhibits strain hardening.

2.2 Stress Concentrations

Stress concentrations can be taken as localized areas within a specimen where stresses noticeably increase. To ensure that the most accurate data can be extracted from the DTT, it would be optimal to have a uniform stress distribution, thus meaning there should be minimal stress concentrations. Unfortunately, it is quite difficult to find the stress concentrations in concrete, as compared to in metal, so there is limited literature on the subject. The non-homogeneous nature of regular concrete causes issues when reading the strains due to the coarse aggregates. However, with UHPC, there are no coarse aggregates, thus overall the UHPC mix is more homogenous. In order to capture the stress concentrations in the concrete specimens, strain gauges will be applied directly to the concrete, much like the method used by Ross and Hamilton III (2010). Generally, the smaller the strain gauge the better it is at detecting strain variations between the mortar, aggregate and the interfacial transition zone (ITZ) (Ross and Hamilton, 2010).

According to their study, strain gauges tend to increase in accuracy as the ratio of the gauge length to aggregate size increases (Ross and Hamilton, 2010). This fundamentally means that the strain gauges that will be used for this research should be sufficiently accurate given that the aggregate size of the J3 UHPC mix is very small.

It is well known that a cylindrical specimen should have the least amount of stress concentrations compared to other shapes when using standard materials, such as metal or wood. So, this study will attempt to show that the addition of metal fibers will not impact the stress concentrations and that the cylinder still has the lowest stress concentrations of the three specimens.

2.3 Strain Hardening

One of the main reasons to use UHPC is because of its increased strengths in both compression and tension. A major factor to the improved tensile strength is a phenomenon called strain hardening. Strain hardening can be defined as the period of loading where the tensile stress exceeds the initial cracking stress. The research conducted by Wille et al. (2014) links four levels of tensile behavior that are exhibited by a cementitious composite. These levels can be described as follows: deflection softening or crack controlling with little enhancement in mechanical properties (level 1), deflection hardening (level 2), tensile strain hardening (level 3), and high energy absorption (level 4). Figure 2.4 shows the graphical representation of the different levels as described by Wille et al. (2014).
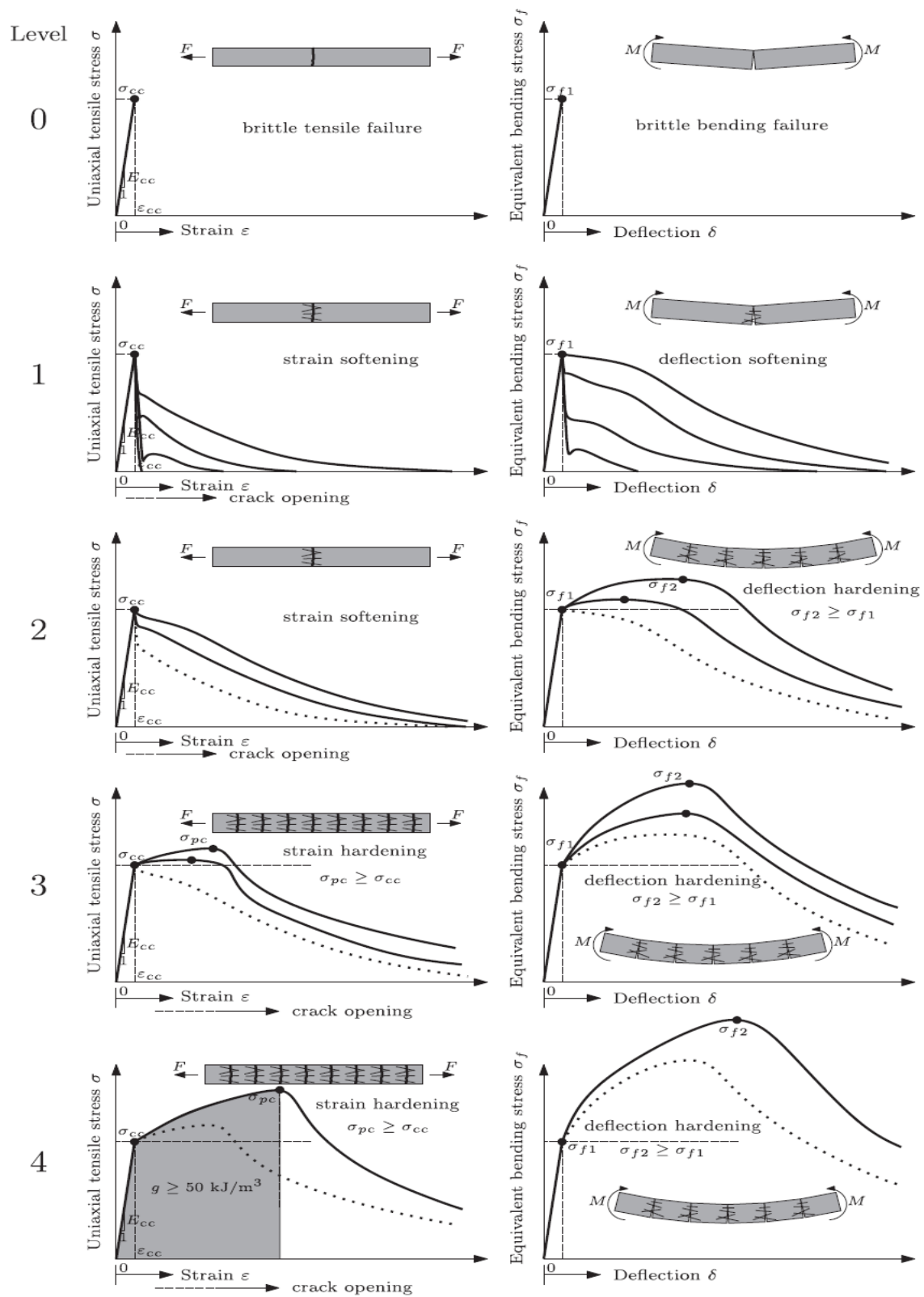
Figure 2.4 Strain Hardening (Wille et al., 2014)

The research found that the tensile level at which the concrete can be placed in is determined by the energy absorption capacity of the concrete (g), and that the best strain hardening happens at a level 4 classification. In order to achieve this level, the concrete should have a $g \geq 50 \frac{kJ}{m^3}$. Typical UHPC mixes with fibers have an energy absorption capacity in the range of 55 to 94 $\frac{kj}{m^3}$, which means that it should exhibit strain hardening. Figure 2.4 also indicates the different behaviors that each level could experience, as seen with the multiple lines. Although Wille et al. (2014) did this research on strain hardening, the optimum fiber content at which it occurs was not found, which is what this research is attempting to find.

Graybeal et al. (2018) provided another report for the FHWA which assessed the properties of multiple UHPC mixes. The mixes ranged from blends manufactured in Europe, in Canada and in the United States. It was stated that the concrete matrix is reinforced with high volumes of fibers, typically greater than or equal to 2% by volume. The UHPC mixes that Graybeal et al. (2018) used created issues when working in remote locations or where the pre-blended dry materials could not be easily shipped. Even though the UHPC mix type was different to that used in this research, the data provided still offers a good comparison. The 14-day compressive strength of each mix is shown in Table 2.5.

Table 2.5 Compressive Strength of Various Specimens (Graybeal et al., 2018)

Age (days)	U-A (ksi)	U-B (ksi)	U-C (ksi)	U-D ([ksi)	U-E (ksi)
14	19.1	18.8	20.2	21.3	17.4

Looking at the tensile stress-strain behavior, Graybeal et al. (2018), determined that for a 2% fiber content, as the strength and the stiffness increases, the nonlinearity prior to failure decreases. This relationship gets further exemplified as the age of the UHPC increases.

The stress-strain response was broken up into three distinct phases: Phase I, Phase II, and Phase III. Phase I refers to the elastic portion of the graph. There is generally an initial linear elastic response until the elastic tension strength is reached. Then comes Phase II, which is referred to as the multiple crack phase. Here, multiple cracks form and are bridged by the fibers. This behavior continues until a single discrete crack forms. In Phase II, the graph can be characterized by any of the following: a plateau effect where the stress remains relatively constant as the strain increases, strain hardening, where the stress increases as the strain increases, or finally a combination of the two. Lastly, Phase III occurs when the primary crack becomes too wide and the fibers get pulled out of the concrete matrix. This can either happen abruptly or gradually, depending on the load and the fiber percentage. A better understanding of these phases is shown in Figure 2.5.
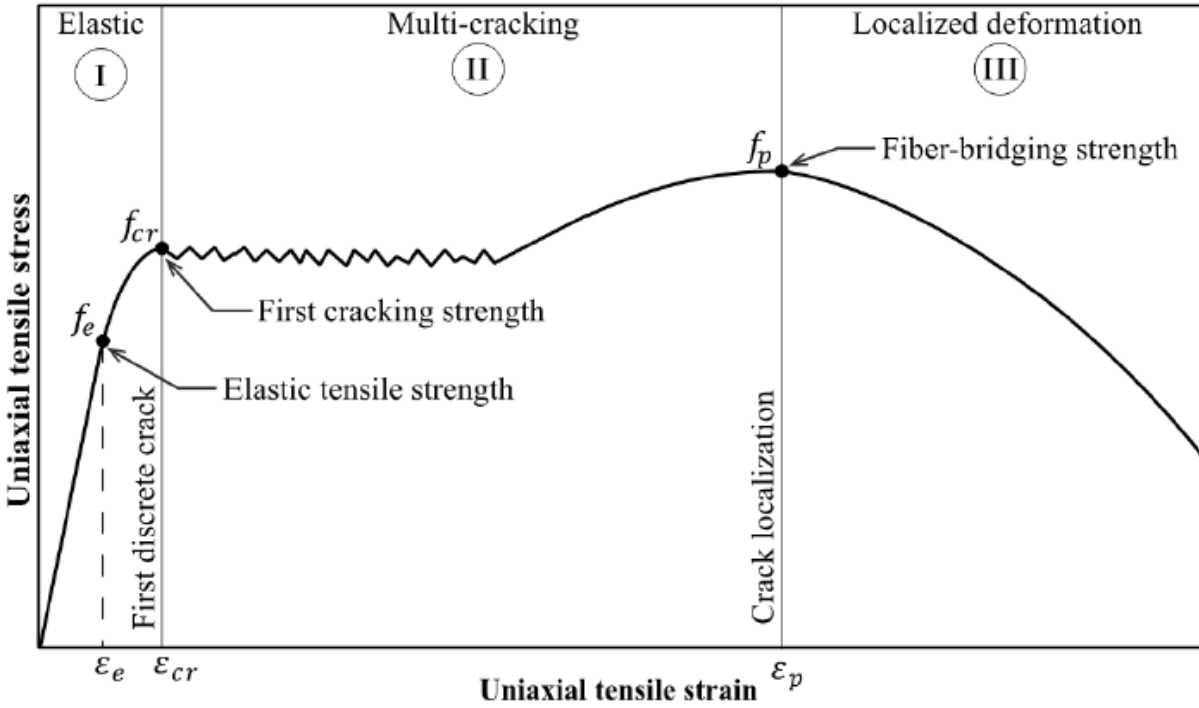
Figure 2.5 Idealized Stress-Strain Curve for UHPC (Graybeal et al., 2018)

Choi et al. (2019) hypothesized that the relationship between the efficiency of steel fibers and the fiber content is a concave parabola. This means that there is a positive trend between the efficiency of the steel fibers and the fiber content when fiber content is low, and after a certain 'tipping' point the relationship becomes negative. A visualization of the steel fibers acting in tension is shown in Figure 2.6.
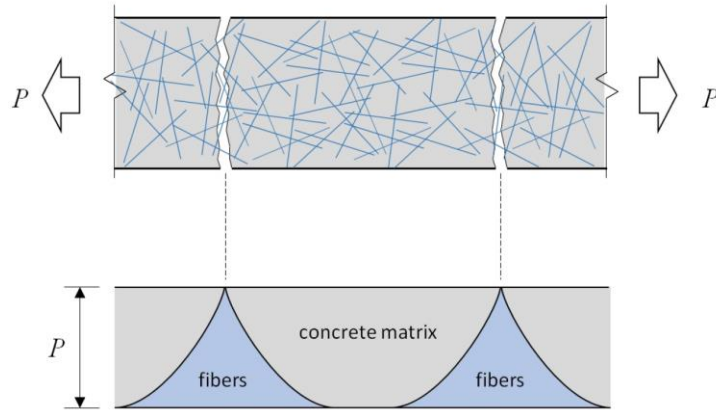
Figure 2.6 Strain Hardening (Choi et al., 2019)

The basic idea for the strain hardening relationship with fibers is that, if there are too many fibers, the concrete matrix cannot bond well with all the fibers. However, if there are too few fibers, then they will not be able to bridge the crack and provide the additional strength. Figure 2.6 also shows the randomness of the orientation of the fibers within the concrete matrix. Not all fibers are bridging the gap, thus not all fibers are adding to the strength gain. This also leads to phenomena of fiber pull-out, which is the when the interfacial bond between the fiber and the concrete matrix fails before the yielding capacity of the fiber. Thus, maintaining the interfacial bond between the fiber and the concrete matrix 'can significantly improve the mechanistic behavior' of the UHPC (Deng et al., 2018).

3 Research Program

3.1 Overview

This section will detail the reasons behind this research and the methods used to determine the tensile strength and behavior of UHPC with different fiber contents. The stress-strain curve is very important for this research, thus careful measures were taken to ensure adequate capturing of the full range of behavior during tension testing. Along with the tensile testing of the UHPC dogbone specimens, the methodology for the stress concentration study will also be outlined. The UHPC mix will follow the non-proprietary J3 mix, which was developed at the University of Oklahoma. An analytical study will also be outlined in this chapter and along with how the analytical study correlates to the experiments.

3.2 Cylindrical Dogbone Test Specimen

As mentioned earlier, the tension test will be done using a cylindrical dogbone specimen. This was chosen as it is believed to provide the best data out of the different specimens while also ensuring that the failure crack will occur in the middle section. The cylindrical dogbone specimens were cast in fabricated hydrostone molds. An aluminum dogbone insert was milled following the dimensions shown in Figure 3.1. The void for the UHPC dogbone was made by casting two halves using the aluminum insert and then clamping them together. To create the first half of the void, the aluminum insert was placed in a box, such that half of the insert was in contact with the hydrostone. Once set, the insert was removed, and the second half was cast. Both the top and bottom halves of the mold were coated in enamel to provide a moisture barrier between the hydrostone forms and the form release. After both halves were adequately coated with enamel and dried, form release was applied, and the halves were clamped together. Four molds were created, three for the testing and one as an extra.
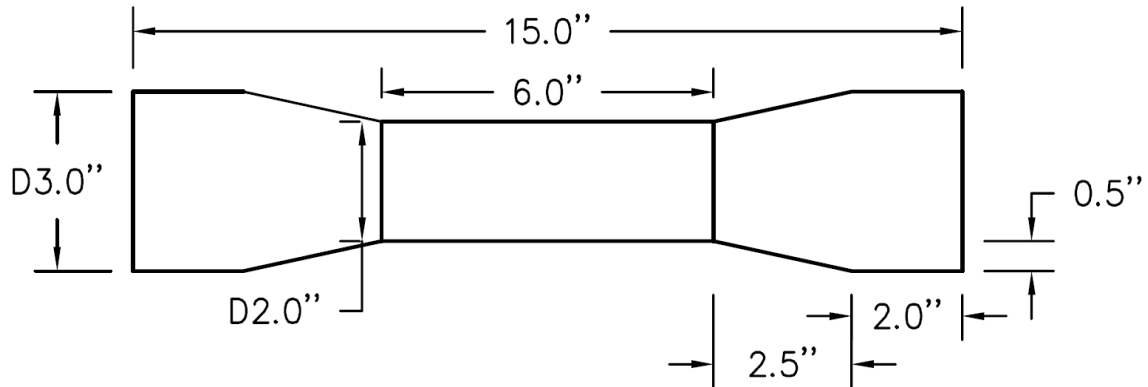
Figure 3.1 Cylindrical Dogbone Dimensions

The cylindrical dogbone specimen was used for both the tension testing and for the stress concentration study. An example the cylindrical dogbone specimen with the aluminum end anchorages is shown in Figure 3.2.

Figure 3.2 Cylindrical Dogbone Specimen with Aluminum Ends

3.3 Cylindrical Test Specimen

Two cylindrical specimens were cast from standard plastic cylinder molds, with dimensions show in Figure 3.3. Accompanying compression specimens were also cast. The two cylindrical specimens were used in the stress concentration study as a comparison to the cylindrical dogbone specimen. An example of the cylinder specimen with the steel end anchorages is shown in Figure 3.4. The methodology and results for the test are outlined in Chapter 5.
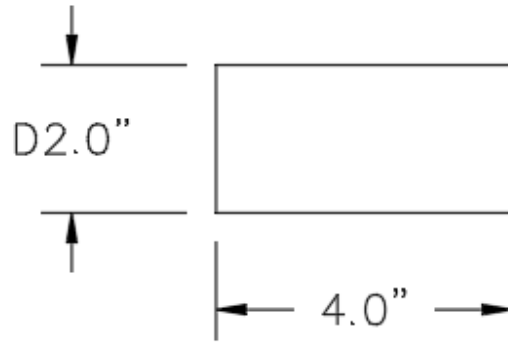
Figure 3.3 Cylinder Specimen

Figure 3.4 Cylinder Specimen with End Anchorages

3.4 FHWA Tension Test Specimen

The two FHWA specimens were cast in a mold with dimensions shown in Figure 3.5. The

FHWA specimen was used to show the stress concentrations at the corners and at the center

while providing a comparison to the cylindrical dogbone and cylinder specimens. An example of

the FHWA specimen with the end anchorages and blocks is shown in Figure 3.6. The

methodology and results for the test are outlined in Chapter 5.
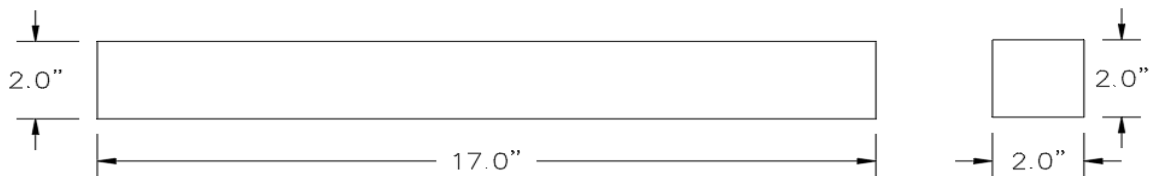
Figure 3.5 FHWA Specimen

Figure 3.6 FHWA Specimen with end anchorages

3.5 Analytical Modeling

The analytical model for the three specimens was done in ANSYS. Each specimen was created using the concrete material with the properties shown in Table 3.1. The models were run in a completely isolated system, so that there were no eccentricities applied to each specimen.

Table 3.1 UHPC properties in ANSYS

Density	155	$\frac{lb}{ft^3}$
Tensile Ultimate Strength	2000	*psi*
Compressive Ultimate Strength	21000	*psi*

The finite element analysis program provided a clear image of where the stress concentrations occurred in each specimen. This was then compared to the actual stress concentration results of the 0% fiber content specimen.

3.6 UPHC Mix for Testing

The proportions of the J3 UHPC mix are shown in Table 3.1, along with the various fiber contents that were tested. It is important to note that the 0%, 1% and 2% mixes have a high range water reducer (HRWR) ounce per hundredweight of 18, whereas for the 4% and 6% mixes, the HRWR was increased from 18 to 23. This increase was necessary to ensure that the mix remained flowable with the increase of the metal fibers. For this J3 UHPC mix, straight fibers (0.2 mm x 13 mm {0.00787 in x 0.5 in}) were used for all fiber percentages. The total volume was set at 0.205 ft^3.

Table 3.2 J3 UHPC Mix with the Various Fiber Contents

Component	Unit	Percentage of Fibers (%)				
		0	**1**	**2**	**4**	**6**
Silica Fumes	*lbs*	1.52	1.51	1.49	1.46	1.43
GGSFB	*lbs*	4.57	4.52	4.48	4.39	4.30
Type I Cement	*lbs*	9.14	9.05	8.96	8.77	8.59
Steel Fibers	*lbs*	0.00	1.00	2.01	4.02	6.03
Masonry Sand	*lbs*	15.23	15.08	14.93	14.62	14.32
Water	*lbs*	3.05	3.02	2.99	2.92	2.86
HRWR	*ml*	81.08*	80.27*	79.46*	99.46**	97.39**

*   - *oz./cwt of 18*

** - *oz./cwt of 23*

The mixing procedure followed the J3 mixing guide, which is shown in Table 3.2. Once mixing was completed, a mortar flow test was conducted following ASTM C1856, to ensure that an adequate flow of at least 6 inches of was achieved for workability. All UHPC specimens were left to set for 24 hours before being removed from the molds and placed in a curing chamber.

Table 3.3 UHPC Mixing Procedure

Step	Description	Time per step (min)	Cumulative Time (min)
1	Mix dry components together in mixer	10	10
2	Gradually add half the HRWR and all the water	2	12
3	Continue mixing	1	13
4	Gradually add remaining HRWR	1	14
5	Continue mixing	2	16
6	Add all of steel fibers*	2	18
7	Continue mixing until mixture appears fully incorporated	3	21

*if no fibers required, continue mixing for allotted time

3.7 Demolding and Heat Curing

The demolding process was very delicate. To demold the cylindrical specimens, a rubber mallet and a putty knife were used. The putty knife was inserted in-between to two halves and

was hit with the mallet until separated. Both the cylindrical dogbone and the cylinders were handled with care, as they had not reached full strength. Once the specimens were removed from the molds, they were placed in a curing chamber for 48 hours. The curing chamber was set to 194 degrees Fahrenheit with an accompanying relative humidity of 95%. This procedure was followed for the remaining fiber contents.

4 Cylindrical Dogbone Specimen Tension Testing

4.1 Overview

It is important to know the tensile capacity of the UHPC material to properly understand the

mechanistic properties. The peak stress and the overall behavior of the UHPC during tension is a

critical factor for materialistic properties and for cost saving methods. This chapter will outline

the procedures behind preparing the specimens for the DTT and present the results from the

tension testing. An analysis of the results is provided in Chapter 7.

4.2 Test Setup and Procedure

4.2.1 Test Setup

Once the cylindrical dogbone specimens were cured following the demolding and curing

procedure, the ends were ground down to be smooth, flat, and parallel. To ensure that the ends

were ground down smooth and parallel, ½ inch spacers were used in the grinding machine. Then

the ends were sandblasted, which ensured better adhesion between the UHPC and the aluminum

end anchorages. Sandblasting makes the ends rough to allow for a greater surface area for

adhesion. The aluminum end anchorage dimensions are shown in Figure 4.1. Once the

cylindrical dogbone specimen ends were completed, the aluminum end anchorages were

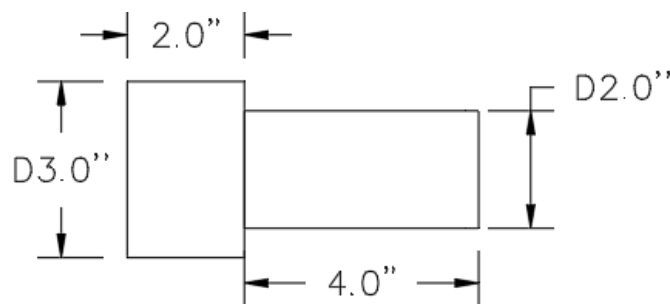sandblasted as well, which again helped to provide a better surface for binding.

Figure 4.1 Aluminum End Anchorages

The gluing apparatus for the cylindrical dogbone specimens is shown in Figure 4.2. A 90-degree bracket was attached to a flat and level surface, then lined with wax paper to ensure that the epoxy would not stick to the brackets. The cylindrical dogbone specimens were laid on the wax paper so that they were flush with the brackets and did not move.

Figure 4.2 Cylindrical Dogbone Specimen Gluing Setup

The aluminum ends had ½ inch spacers to ensure that the ends were level when gluing them against the cylindrical dogbone specimen. JB ClearWeld was used as the adhesive and was placed on both the aluminum ends and the dogbone ends, which were then manually squeezed together and held for one minute before being allowed to set for 24 hours.

JB ClearWeld was chosen as the adhesive because of its high bonding strength and its ease of application. With a tensile strength stated at 3,900 psi, JB ClearWeld provided adequate bond strength for tension testing of the UHPC material, which was expected to be less than 3,000 psi.

Once the aluminum ends were set, the LVDT brackets were then attached. The initial setup had 90-degree brackets attached to the 2-inch diameter middle section of the dogbone via a hose

clamp, as shown in Figure 4.3. This led to a shorter gauge length and an inability to correctly

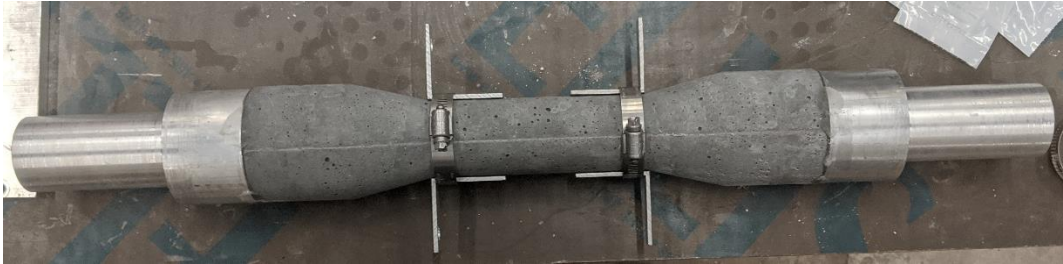capture the crack. Upon testing with this setup and seeing the issues, a new method was used.

Figure 4.3 Hose-clamped LVDT Brackets

The new method that was used to attach the LVDTs is shown in Figures 4.4 and 4.5. Two 6-

inch spacers were created for each cylindrical dogbone to ensure that the LVDT brackets were

equally spaced, thus ensuring the similar gauge lengths. The 90-degree brackets were bent in

such a way that, one side sat flat on the tapered section of the dogbone, while the other side was

perpendicular to the cylindrical dogbone specimen. Then the brackets were glued using JB

ClearWeld and held in place with painters' tape, as shown in Figure 4.5.
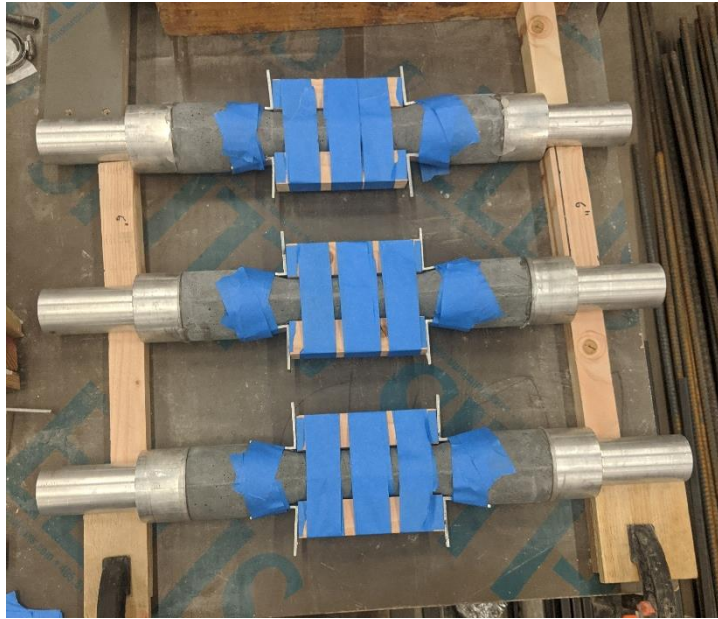
Figure 4.4 Spacer for LVDT Brackets

Figure 4.5 Drying Setup for LVDT Brackets

The specimens were left to cure for one day before the painters' tape was removed and the cylindrical dogbone specimens were ready to be tested.

4.2.2 Test Procedure

The tension testing was conducted and followed the steps outlined in ASTM C1583. Two LVDTs, named as 'LVDT 1' and 'LVDT 2' were added to the brackets to measure the extension of each specimen. The two LVDTs were placed diametrically opposite from each other to capture an average of the specimen's extension. Figure 4.6 shows the cylindrical dogbone specimen setup in the Baldwin (the machine used for the DTT). Ideally a displacement-controlled test would provide the best test, however due to the limitations of the Baldwin, a quasi-load-controlled test was conducted. Throughout the testing procedure, the loading rate was set on the Baldwin at 40 lb/s.

Figure 4.6 Cylindrical Dogbone in Baldwin with LVDTs

The cylindrical dogbone was placed into the Baldwin as carefully as possible, ensuring that it was vertical. Any eccentricity experienced by the specimen would cause skewed results and add unwanted bending to the specimen.

The compression test followed the steps outlined in ASTM C39. For each fiber content, three 3 inch x 6 inch cylinders were ground to ensure flat and parallel surfaces before being placed into the Forney for the compression test. The Forney was set to preload up to 55,000 lbf with a ramp rate of 150 psi/s.

4.3 Test Results

Following the tests performed on the cylindrical dogbone specimen, the results are shown in Table 4.1. For each test, the gauge lengths of both LVDTs were measured along with the post

cracking failure area, which is shown in Table 4.1. To find the failure area, three diameters were measured around the failure and averages, then the failure area for each specimen was calculated.

Table 4.1 Gauge length and Failure Area of the Different Fiber Contents

Fiber content	Average Gauge length [in]						Failure area [in^2]		
	LVDT 1			LVDT 2			Test 1	Test 2	Test 3
	Test 1	*Test 2*	*Test 3*	*Test 1*	*Test 2*	*Test 3*			
0%	5.28	5.21	5.29	5.37	5.33	5.38	3.20	3.20	3.24
1%	5.29	5.24	5.31	5.37	5.39	5.35	3.33	3.35	3.33
2%	5.29	5.29	5.30	5.37	5.34	5.36	3.20	3.20	3.20
4%	5.30	5.27	5.31	5.27	5.27	5.30	3.20	3.21	3.20
6%	5.40	5.42	5.37	5.37	5.41	5.39	3.31	3.17	3.23

After testing each fiber content and measuring the failure area, the peak tensile strength was determined for each test, which is shown in Table 4.2, along with the accompanying compressive strengths.

Table 4.2 Compressive and Peak Tensile Strength of the Different Fiber Contents

Fiber content	Compression strength (f'$_c$) [psi]	Tensile Strength [psi]		
		Test 1	Test 2	Test 3
0%	16,820	360	340	360
1%	17,100	470	940	720
2%	18,880	730	670	860
4%	18,350	950	1,060	880
6%	20,070	1,090	890	700

The ideal location for the crack to occur is at or near the center of the cylindrical dogbone.
Figure 4.7 shows an example of the ideal location for the crack. When fibers are introduced,
multiple cracks could form due to the steel fibers bridging the initial crack, as shown in Figure
4.8.

Figure 4.7 Crack Formation on Cylindrical Dogbone Specimen

Figure 4.8 Multiple Crack Formation

Figure 4.9 shows the progression of the crack formation. The specimen initially cracks, as
shown in Figure 4.9 (a), and then as the load is continually applied, the force is transferred from
the concrete to the fibers bridging the gap, as shown in Figure 4.9 (b). Finally, the fibers are not
long enough to bridge the gap, thus the specimen completely separates and fails, as shown in
Figure 4.9 (c).

(a)   (b)   (c)

Figure 4.9 (a) Initial Crack Location, (b) Fibers Bridging Crack, (c) Post Crack

Following the test, the load versus displacement data was collected and graphed as shown in
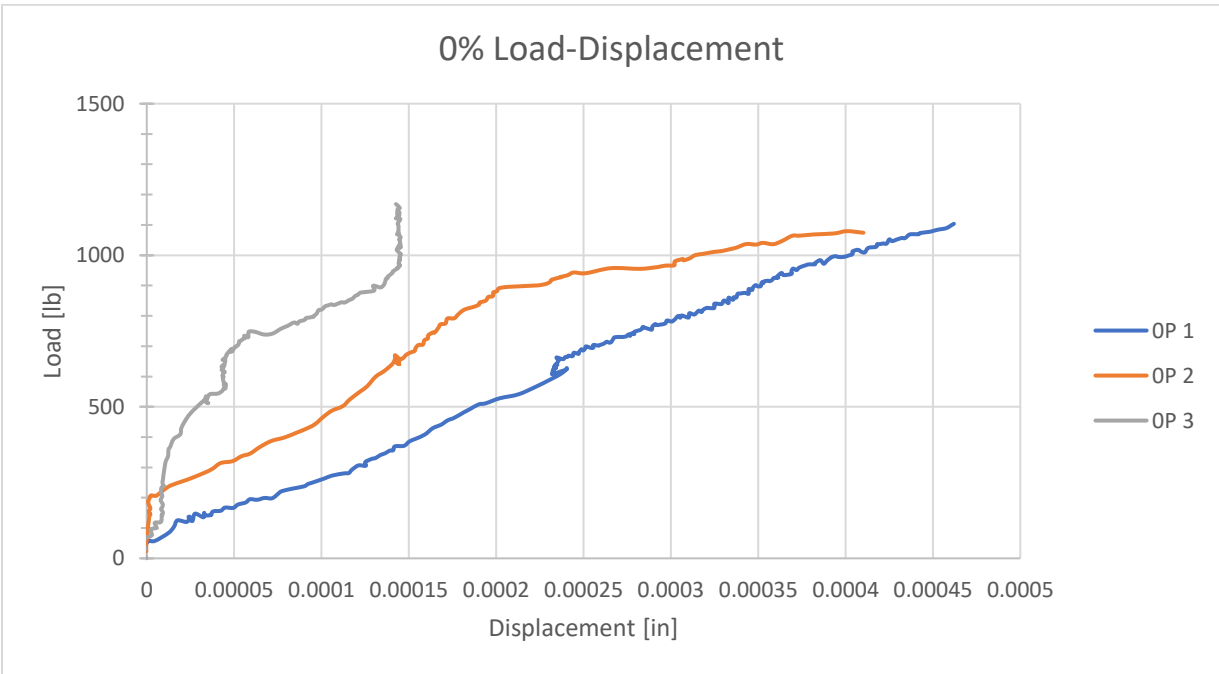
Figures 4.10 through 4.14.
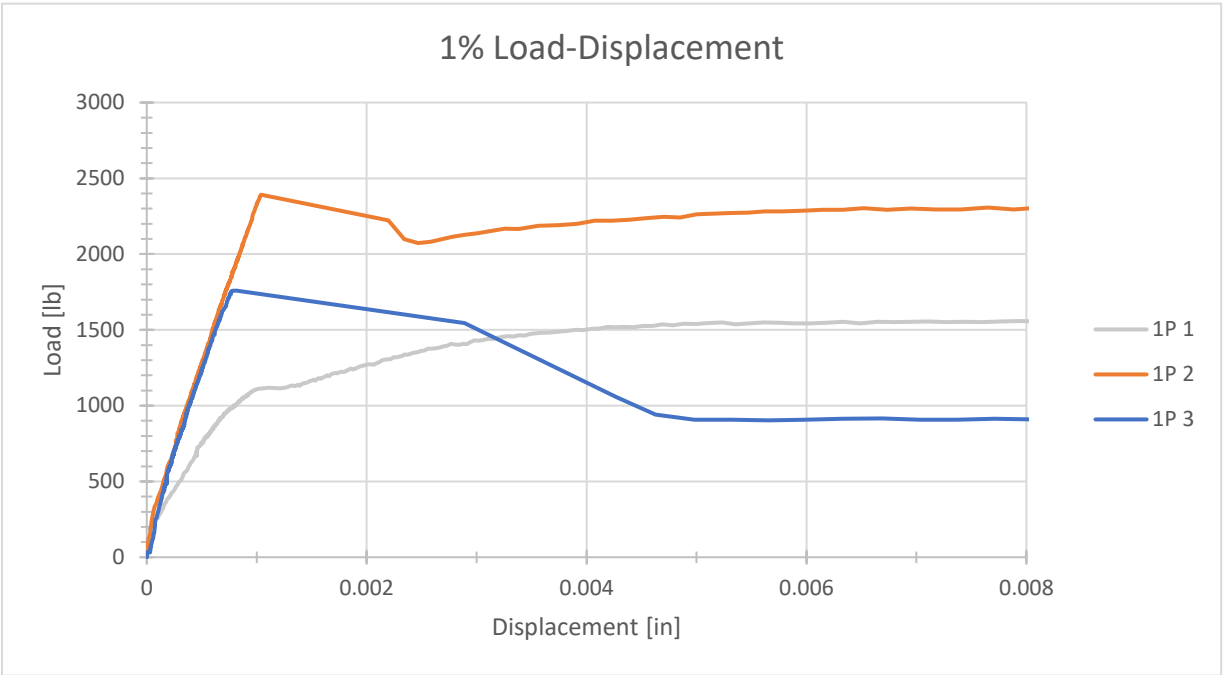

Figure 4.10 0% Load vs Displacement Graph
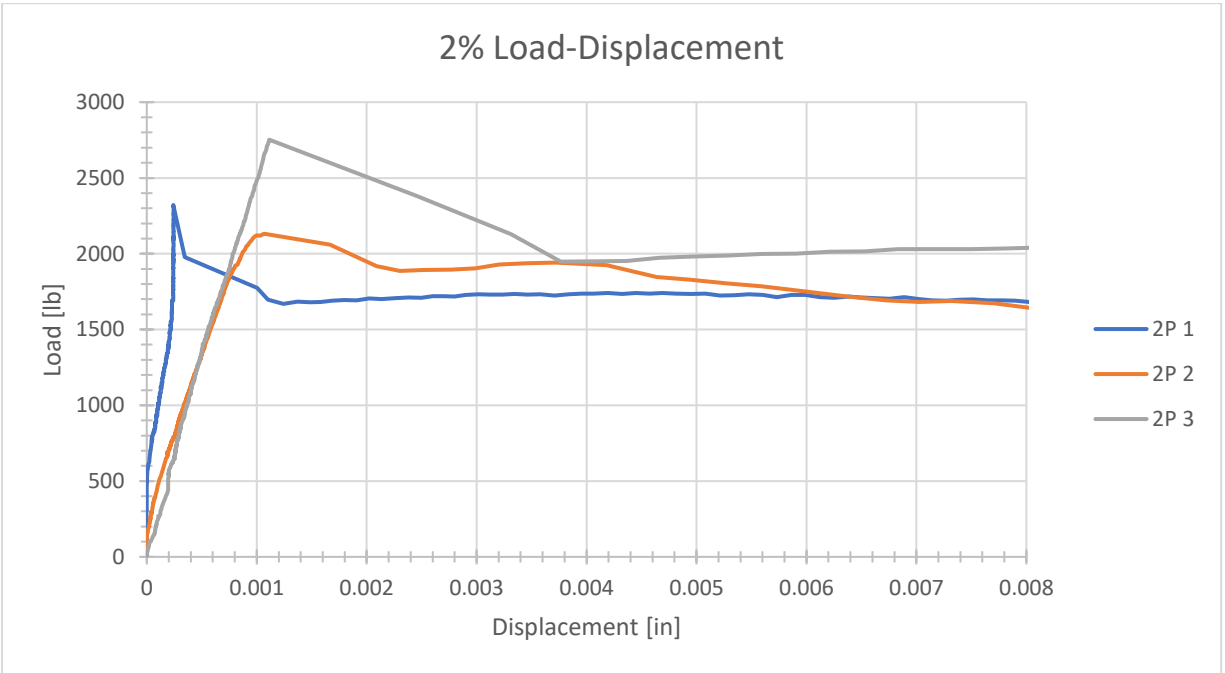
Figure 4.11 1% Load vs Displacement Graph

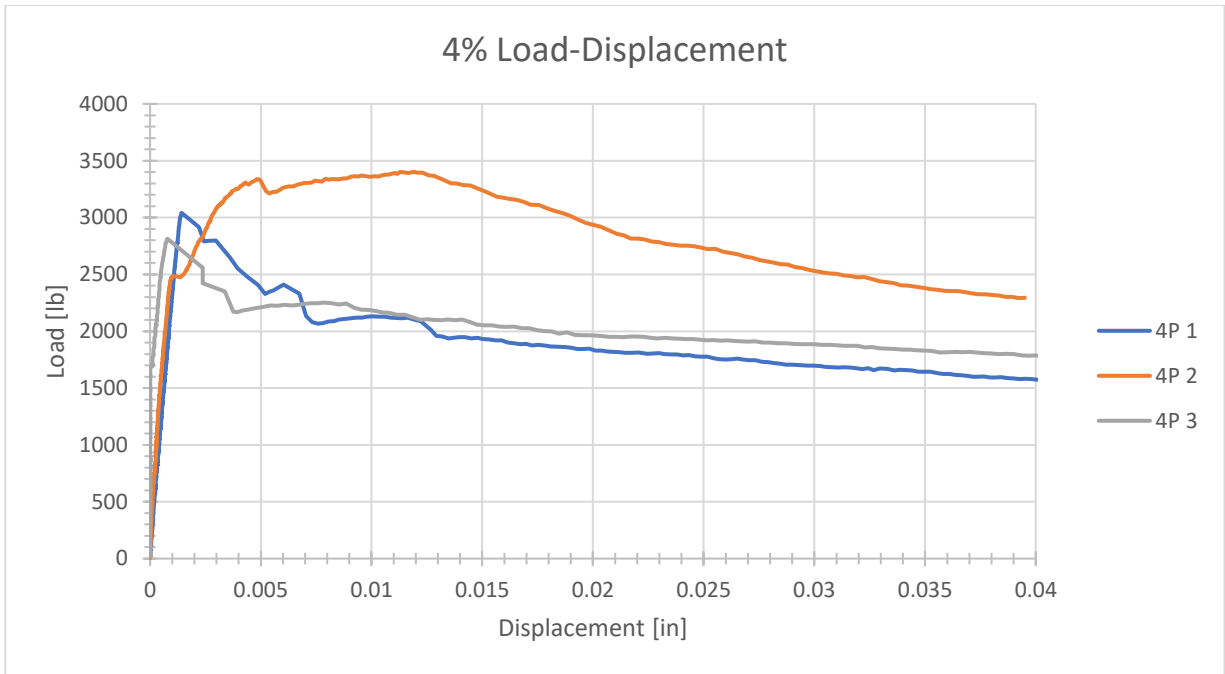*Figure 4.12 2% Load vs Displacement Graph*
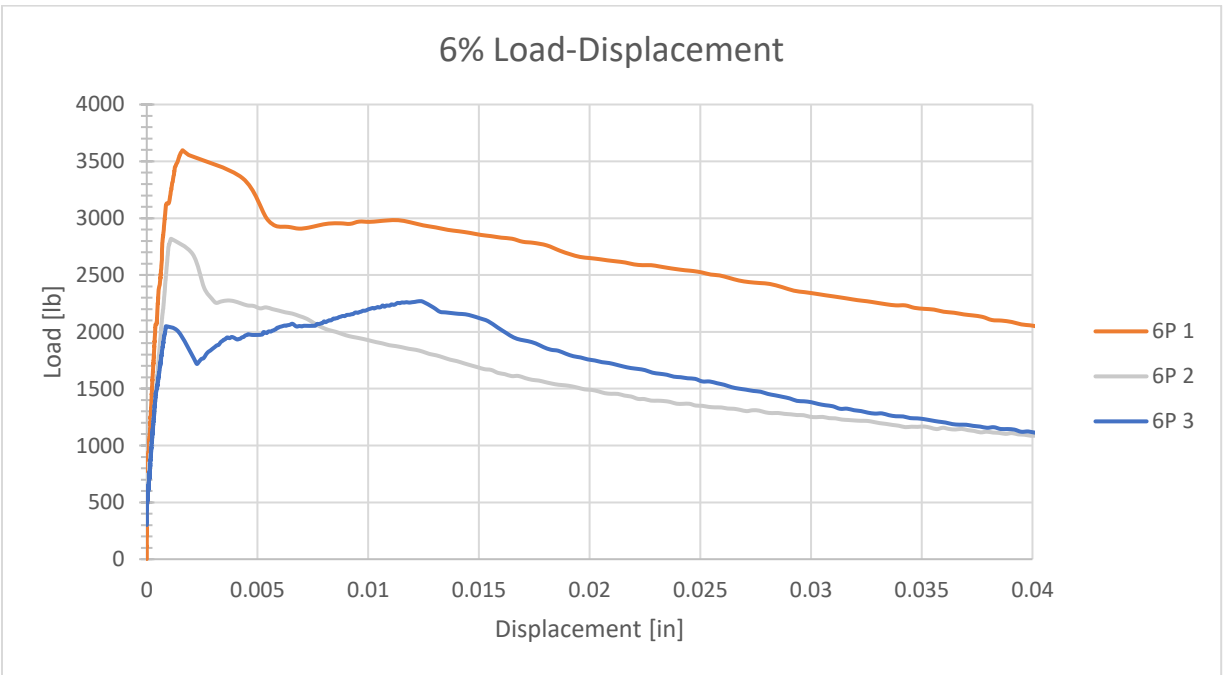
Figure 4.13 4% Load vs Displacement Graph

Figure 4.14 6% Load vs Displacement Graph

5 Stress Distribution Study

5.1 Overview

The following chapter details a study of the stress distribution within three potential UHPC

tension test specimens – the cylindrical dogbone specimen, a cylindrical specimen, and the

FHWA proposed specimen. The stress distribution is critical in evaluating the accuracy and

repeatability of potential UHPC tension test methodologies. The J3 UHPC mix without fibers

was used to compare the stress distributions and potential stress concentrations within the

different specimen types. The mixing procedure was the same as previously stated in Section 3.6.

Once mixed, two specimens of the cylindrical dogbone, two 2 inch x 4 inch cylinders and two 2

inch x 2 inch x 17 inch FHWA prisms were created. To ensure continuity and precision in data

collection, accompanying compression specimens were also cast. All specimens followed the

same curing process as the previous cylindrical dogbone tensile test. Once cured for 48 hours,

strain gauges were attached to each specimen at critical locations to evaluate the stress

distributions under load. The gauge length of the strain gauges was 6 mm with a gauge factor and

resistance of 2.11% and 350 Ω, respectively. The process to prepare all the specimens consisted

of the following:

1. Epoxy area where strain gauges were to be located

    a. This step was performed in order to fill in any voids under the strain

        gauges

2. Sand the epoxied areas using 200 grit sandpaper

    a. This step helped to smooth the area for the strain gauges

3. Clean the epoxied areas with acetone, an acid and a base

4. Attach the strain gauges into their locations using clear tape

5.   Lift the tape and apply the strain gauge epoxy

6.   Allow the epoxy to fully dry before completely removing tape

An analysis of the results is provided in Chapter 7.

5.2 Cylindrical Dogbone Specimen

For the cylindrical dogbone specimen, a total of eight strain gauges were used. The first four were placed in the center of the specimen and diametrically opposed from one another. This arrangement meant that the strain gauges could capture data from all four quadrants around the cylinder. The second set of four strain gauges were placed at the boundary where the tapered section meets the central section, as shown in Figure 5.1. In addition to this, the last four strain gauges were placed directly above the first four, in order to better capture the differences between the two locations.

Figure 5.1 Strain Gauge Location on Cylindrical Dogbone Specimen

Once the strain gauges were attached, the cylindrical dogbone specimen was placed in the

Baldwin and tested in a similar manner to the tensile capacity test as previously discussed in

Chapter 4. The results of the strains in the center section and the boundary of the tapered section
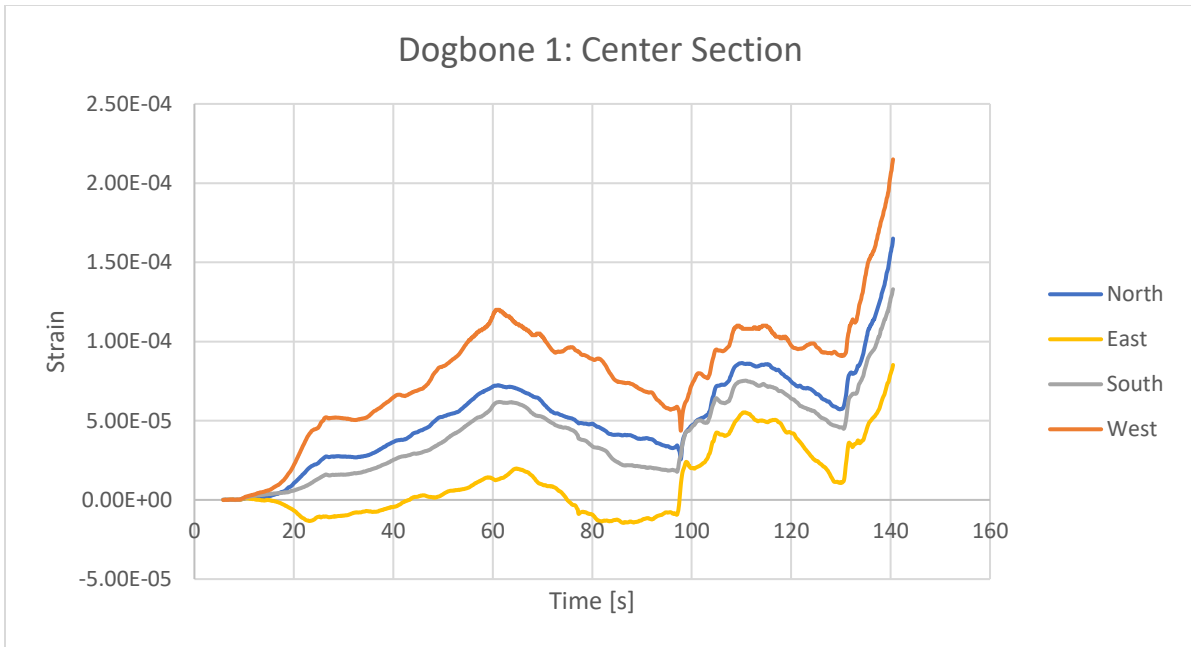
are shown in Figure 5.2 to Figure 5.5.

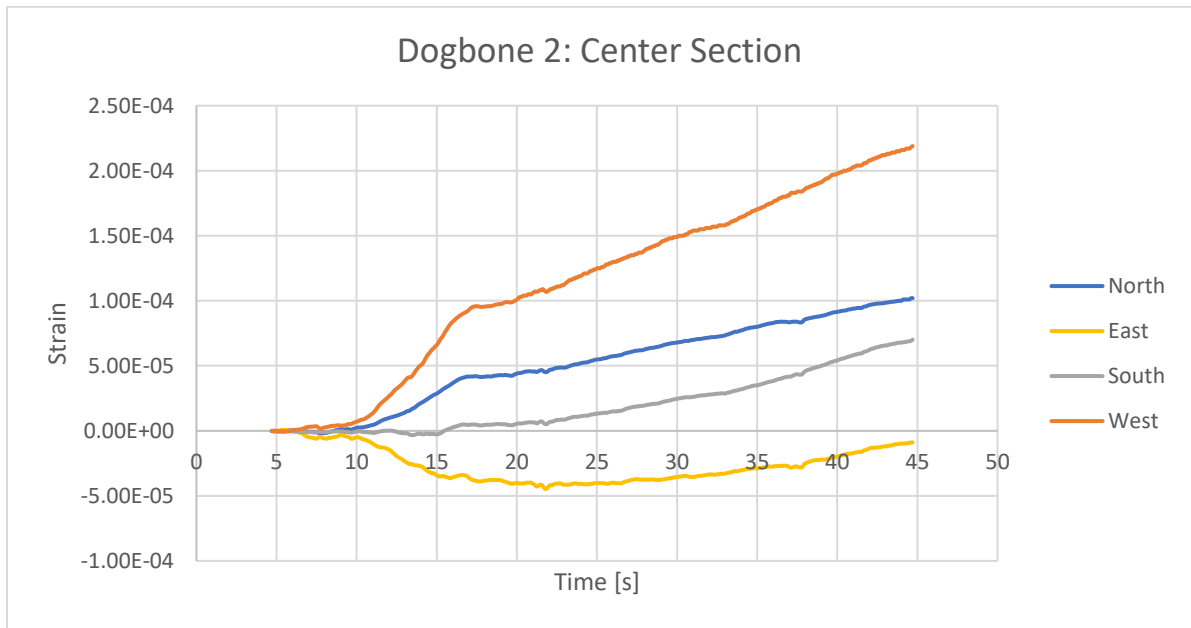*Figure 5.2 Strain Gauge data for Dogbone 1 at Center*

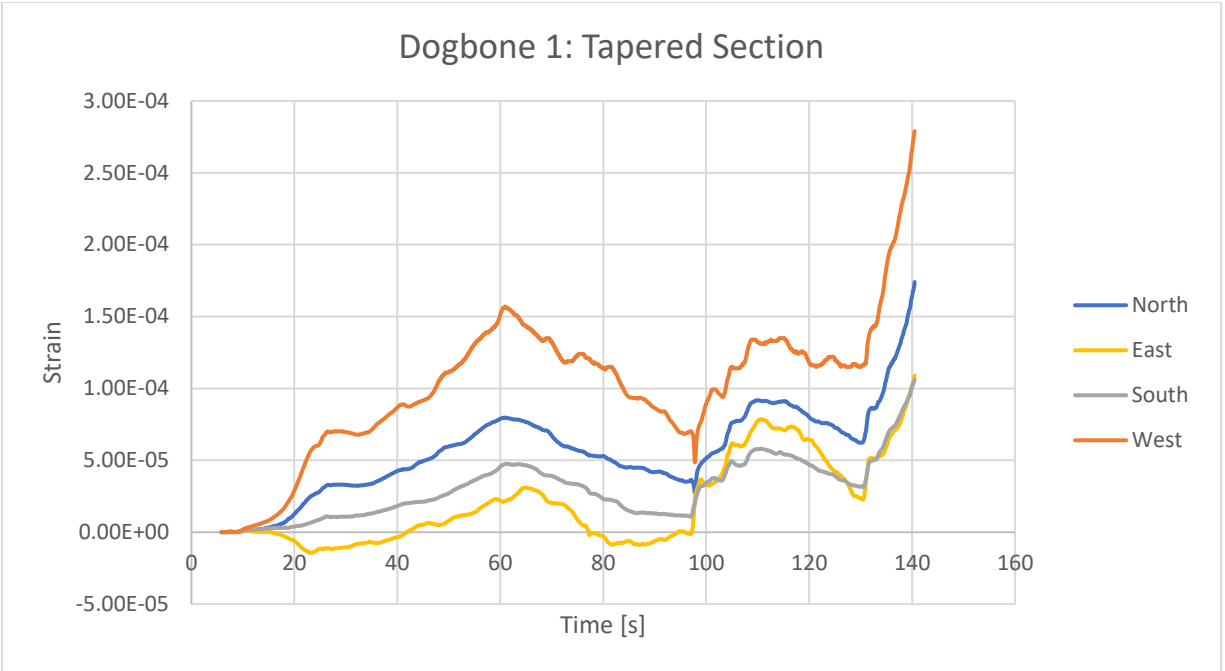*Figure 5.3 Strain Gauge data for Dogbone 2 at Center*

Figure 5.4 Strain Gauge data for Dogbone 1 at Tapered Section
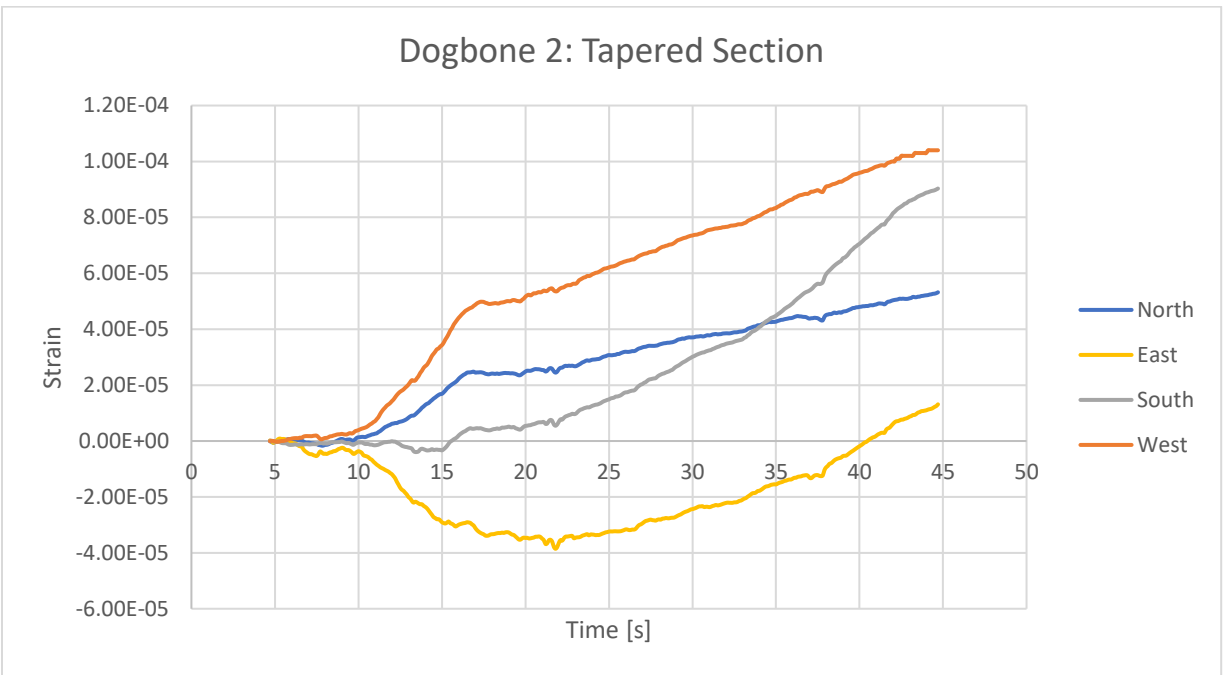

Figure 5.5 Strain Gauge data for Dogbone 2 at Tapered Section

5.3 Cylindrical Specimen

Once the cylinders were fully cured, they were ground down until smooth and flat. Both the UHPC cylinder ends and the steel ends were then sandblasted prior to being epoxied to improve bond.

For the 2 inch x 4 inch cylinders, only four strain gauges were used. They were placed in the center of the specimen, diametrically opposed from each other, thus having a strain gauge in each quadrant. This is the same locations as the first four strain gauges for the cylindrical dogbone specimens. One of the locations for the strain gauges on the cylinder is shown in Figure 5.6. The other strain gauges were placed in such a way, that again, all four quadrants were captured.

Figure 5.6 Strain Gauge Location for Cylindrical Specimen

After everything was fully cured, the cylinder was placed in the Baldwin and the experiment was started. The cylinders followed the same loading rate as the cylindrical dogbone. The results from the experiment are shown in Figures 5.7 and 5.8 below.
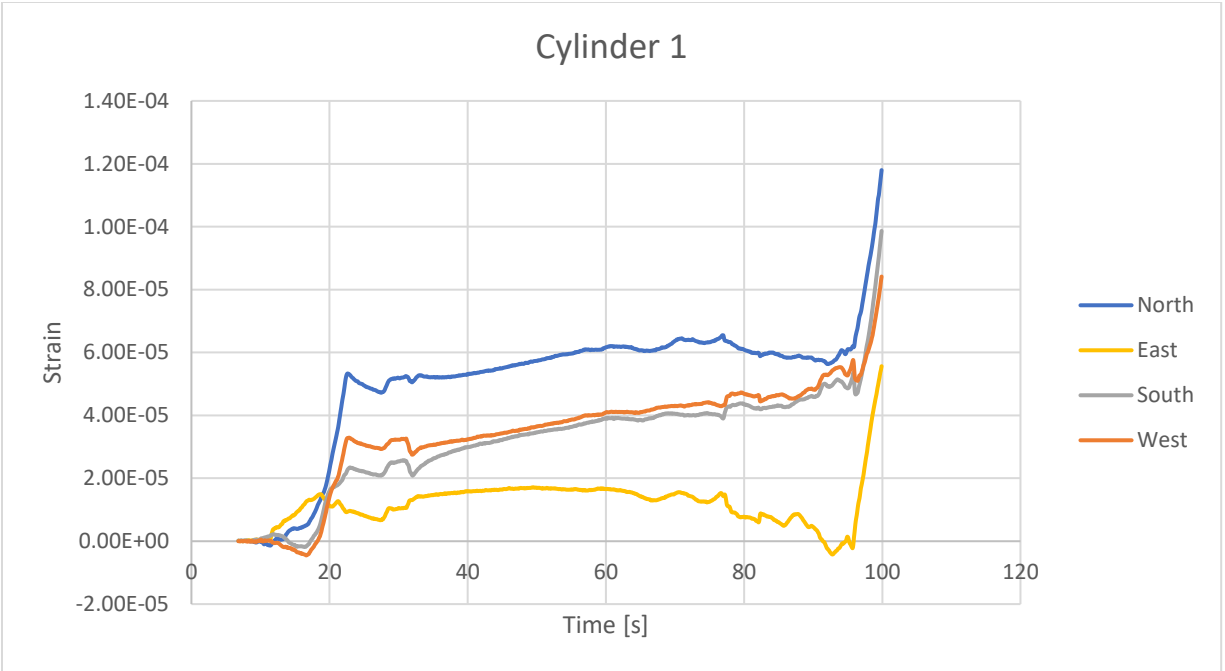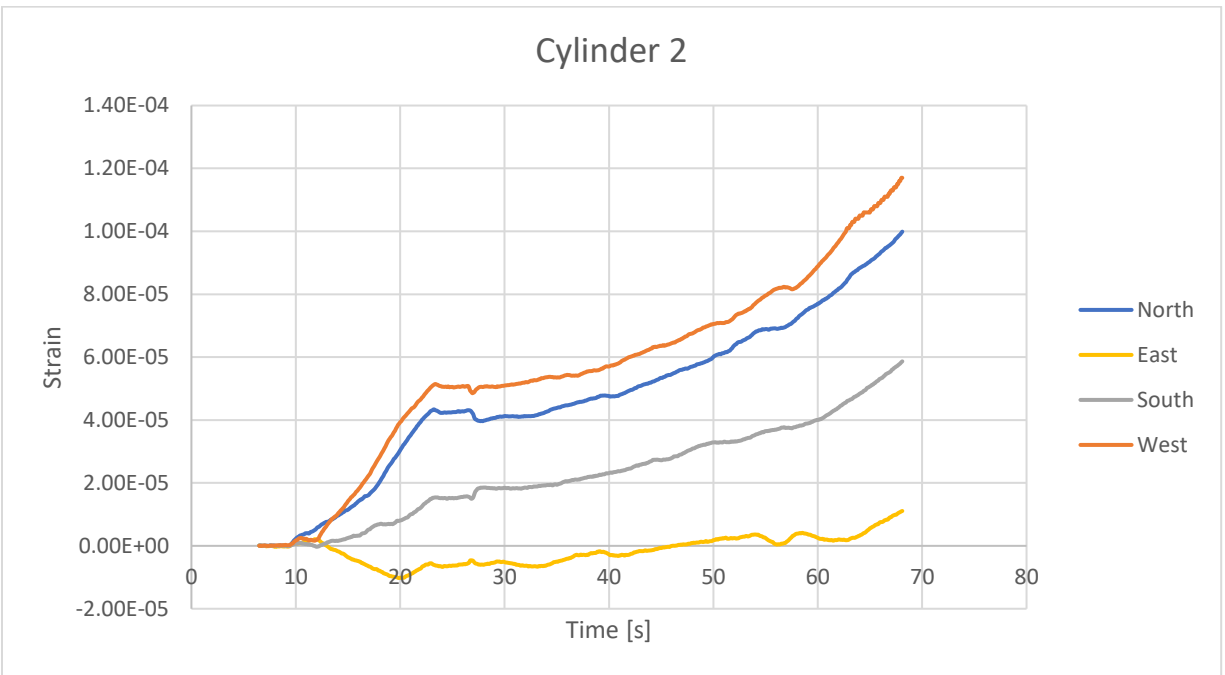
Figure 5.7 Strain Gauge data for Cylinder 1

Figure 5.8 Strain Gauge data for Cylinder 2

5.4 FHWA Specimen

The FHWA specimen followed the same processes as the other two specimens. After the specimen was cured in the curing chamber, two of the sides were sandblasted along with the aluminum ends. A completed specimen with the aluminum ends in place is shown in Figure 5.9. There were 4 end anchorages that were epoxied onto the sandblasted sides of the FHWA specimen. A spacer was added during the gluing process to ensure that the ends were parallel to each other. This same spacer was also used during testing to avoid unnecessary rotation of the ends.

Figure 5.9 Ends Epoxied on FHWA Specimen

The specimen also had eight strain gauges to study the stress distribution. Again, the first four were placed at the center of the specimen, so that the ends did not have any effect on the stress distribution. The remaining four were placed at the corners of the prism and in line with the first four, as shown in Figure 5.10. The other strain gauges were placed in the same locations on the other faces.
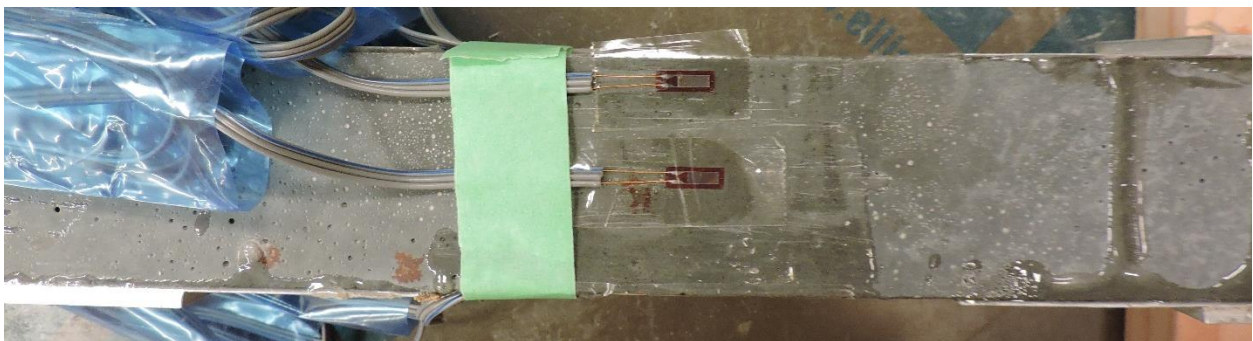

Figure 5.10 Strain Location on FHWA Specimen

Following the test, the results for the middle strain gauges and the corner strain gauges for the first specimen are shown in Figures 5.11 and 5.12, respectively. The middle strain gauges and the corner strain gauges for the second specimen are shown in Figures 5.13 and 5.14, respectively.
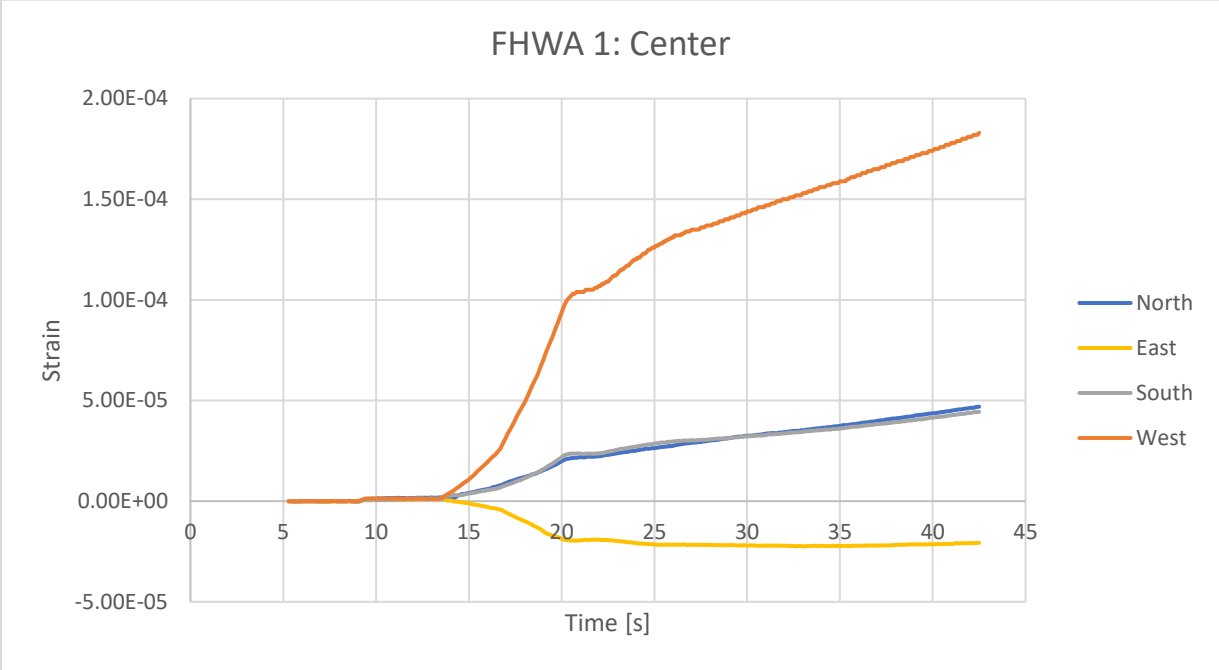

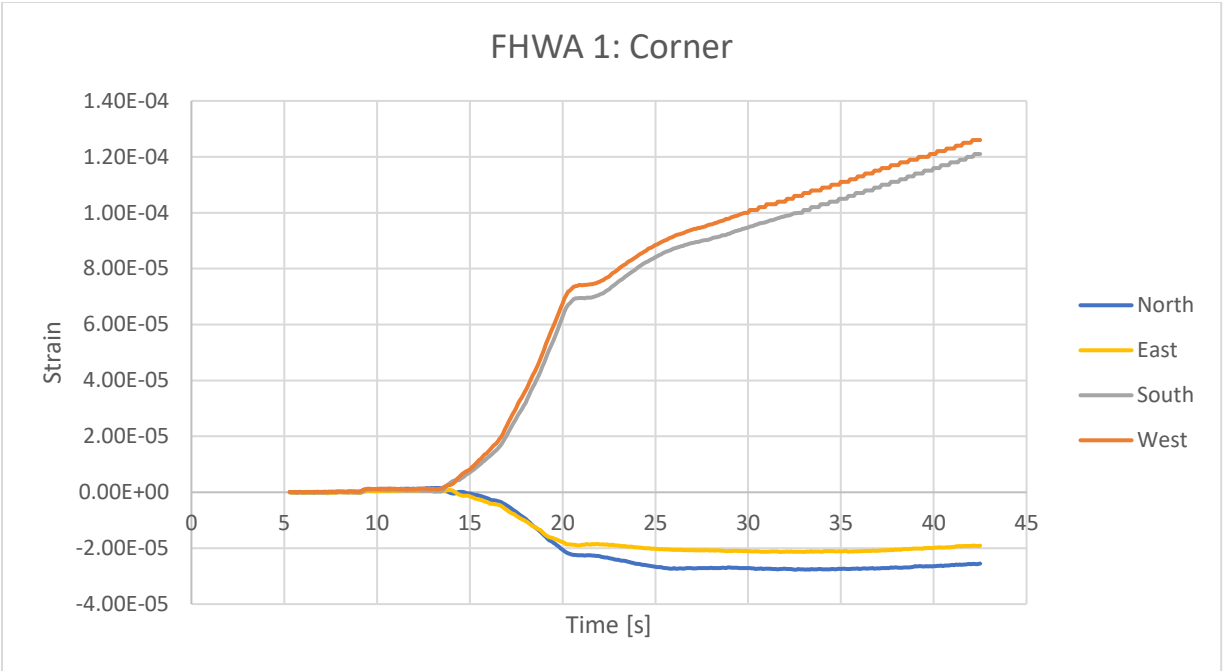*Figure 5.11 Strain Gauge data for FHWA 1 at Center*
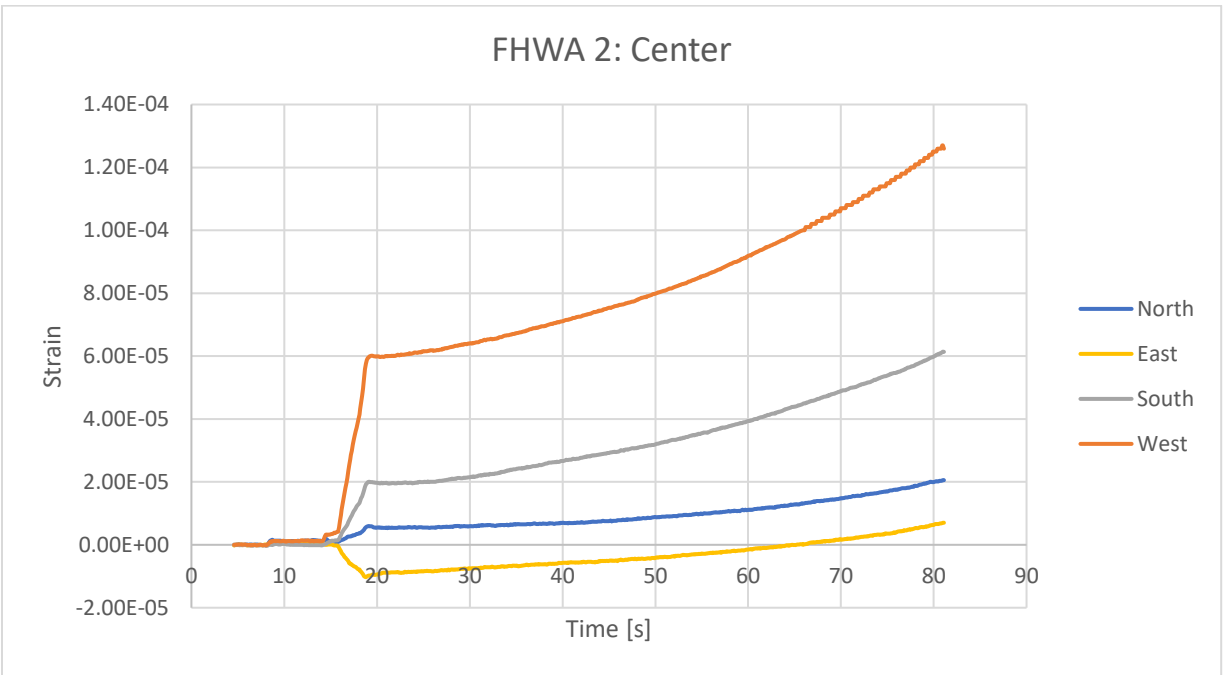
Figure 5.12 Gauge data for FHWA 1 at Corner

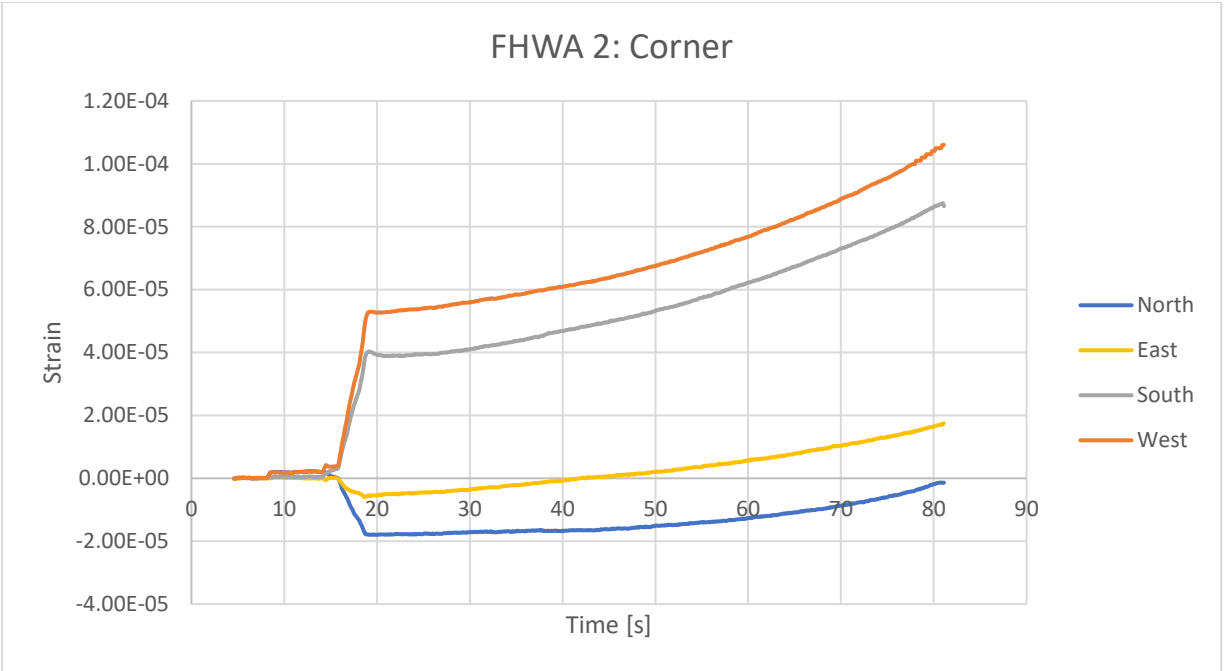*Figure 5.13 Gauge data for FHWA 2 at Center*

Figure 5.14 Gauge data for Second FHWA 2 at Corner

6 Analytical Study

6.1 Overview

The following chapter details the analytical study that was conducted on the three potential

UHPC tension test specimens detailed in Chapter 5. A finite element model was created for each

specimen type using ANSYS. Utilizing the properties outlined in Section 3.5, a detailed model

showing how the stresses change within the different specimens was created for each specimen

type. It is important to understand where stress concentrations potentially occur as this has an

impact on the accuracy and repeatability of each testing methodology. An analysis of the results

is provided in Chapter 7.

6.2 ANSYS Programming

To ensure that each model could be effectively compared to one another, all forces and fixed

supports were modeled the same for every specimen. Each specimen was oriented vertically in

the program to match the actual test. Each model of the specimens followed the same design

procedure. A fixed support was placed on one end so that there was no movement, with a load

being applied at the opposite end. Both the cylindrical dogbone and the cylinder had the fixed

support applied to the face, as shown in Figure 6.1. This location best represents how the

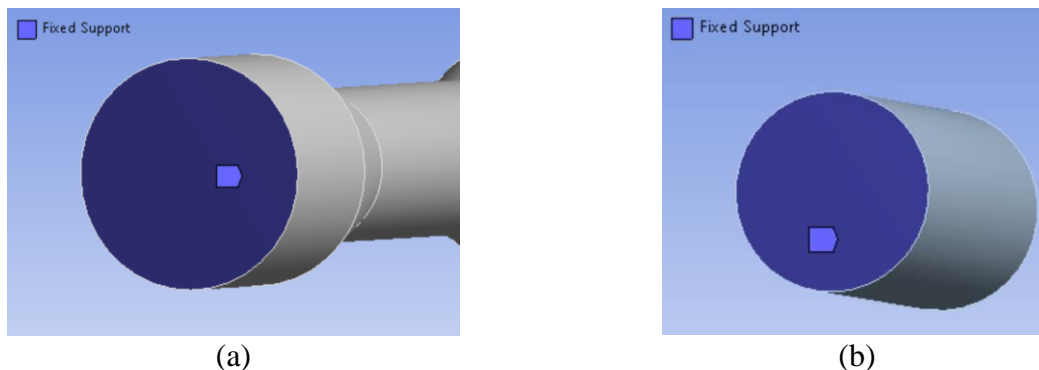physical specimen experienced the applied force from the aluminum attachments.

(a)   (b)

Figure 6.1 (a) Fixed Support on Cylindrical Dogbone (b) Fixed Support of Cylinder

For the FHWA specimen, the fixed support was applied to the sides, to best model exactly how the test was accomplished. Figure 6.2 shows how the fixed supports were applied to the FHWA specimen. The fixed support shown in Figure 6.2 (a) was also applied to the opposite side. This approach most accurately models the actual support conditions as shown in Figure 6.2 (b).
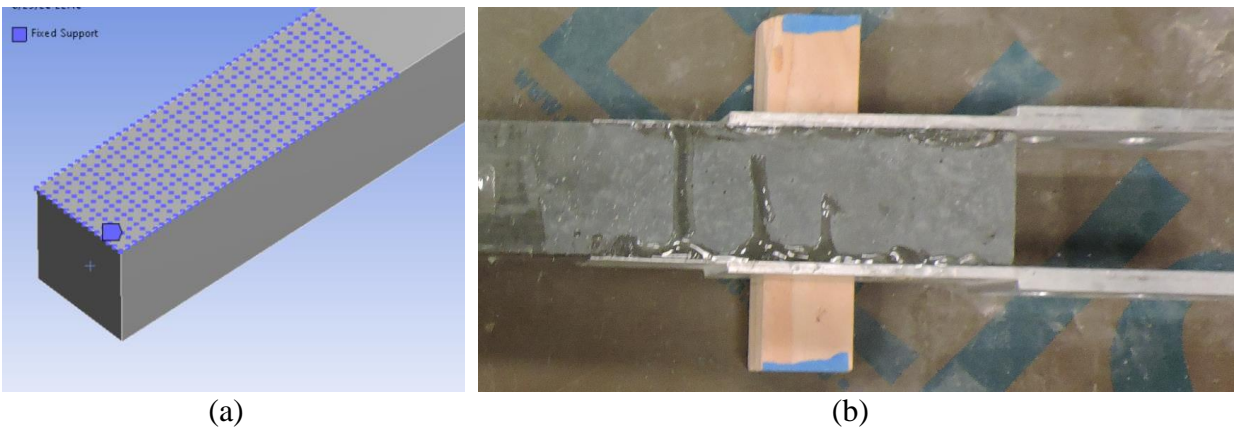

(a)   (b)

Figure 6.2 (a) Fixed Support of FHWA in ANSYS (b) Supports in Physical Test

Due to the limitations of the student version of ANSYS, the mesh sizing was limited to 0.3 inches, with 32,000 nodes and elements. The analysis was completed using a static structural model with concrete and element type was Solid186.

From the tension test results, the average 0% fiber content stress at failure was found to be around 280 psi. Therefore, for this analytical investigation, a constant stress of 350 psi was applied. The increase was done to aid in recognizing stress variations within each specimen type. The stress was then divided by the cross-sectional area of the middle of each specimen to find the required applied load. For both the cylindrical dogbone and the cylinder, a force of 1,099 lb was applied, whereas for the FHWA specimen, the force was 1,400 lb due to the larger cross-sectional area.

6.3 Results

Following the programming, the models were run in ANSYS and the following results were found. Figure 6.3 shows the stress distributions of the cylindrical dogbone specimen. The stress distributions for the cylinder are shown in Figures 6.4, while that of the FHWA specimen is shown in Figures 6.5.
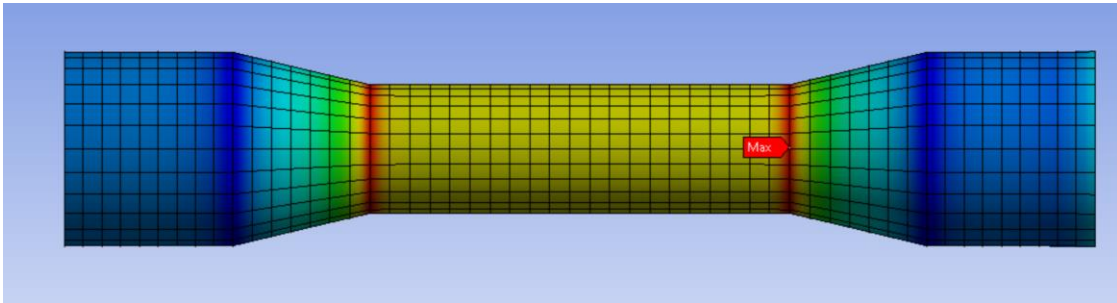

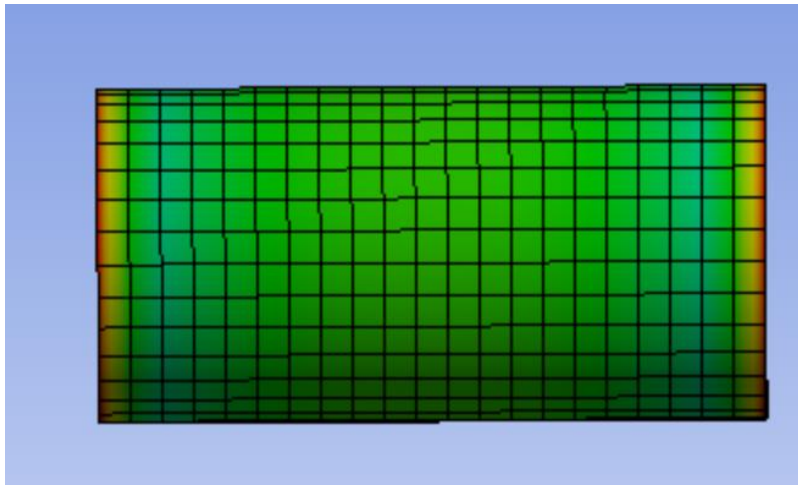*Figure 6.3 ANSYS Model of the Cylindrical Dogbone*
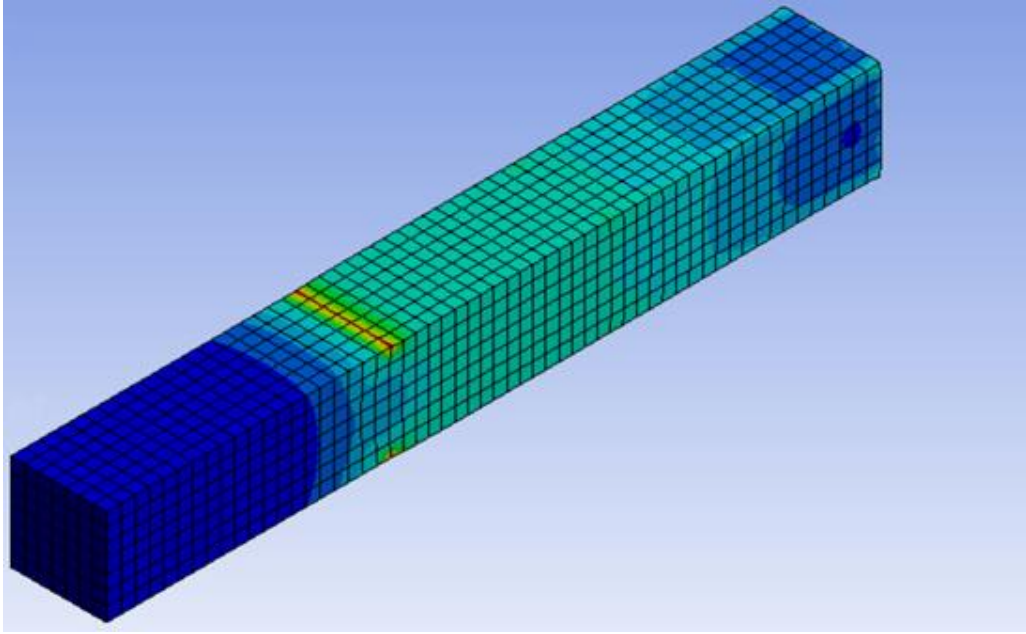

Figure 6.4 ANSYS Model of the Cylinder

Figure 6.5 ANSYS Model of the FHWA Specimen

7 Analysis of Results

7.1 Overview

Chapter 7 details the analysis of the results, mainly focusing on the tension capacity and the post-cracking behavior of the cylindrical dogbone, and lastly the stress distribution of all three specimen types. Understanding the differences between the different fiber contents and how the post-crack behavior occurs is critical in improving the use of UHPC throughout all facets of construction. The analysis of the stress distribution is crucial in understanding the behaviors of the different specimen types.

7.2 Tension Capacity

This section contains an analysis of the tension capacity test results. The stress was normalized by the respective average compressive strengths in order to provide a better comparison between the different fiber contents. Figure 7.1 shows the behavior of the J3 UHPC mix with 0% fibers. From the graph, it is clear that the stress and the strain come to an abrupt stop. This behavior is due to there being no fibers to bridge the initial crack. The 0% test served as a control in comparison to traditional concrete and to show the effects of fiber content in UHPC. As shown in Figure 7.1, the three tests were quite different from each other. One of the main reasons for this was the slipping between the grips in the Baldwin and the aluminum ends. However, for the most part, the overall behavior was mostly linear up to failure.

Normalized Stress-Strain for 0%
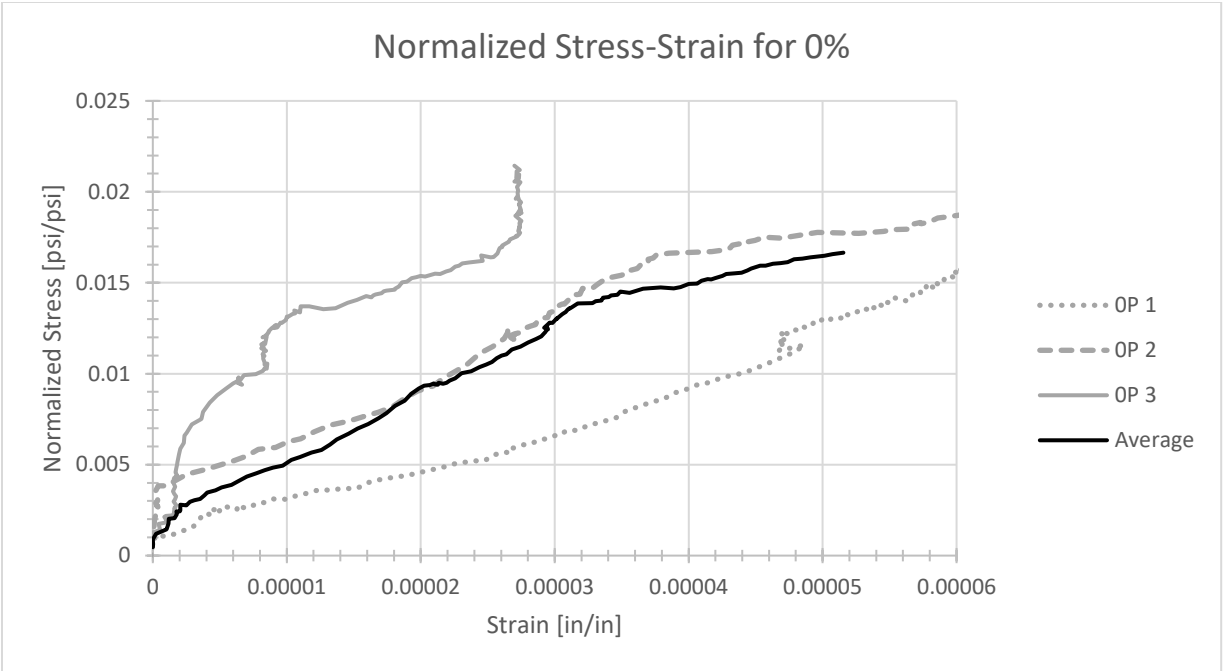
Figure 7.1 Normalized Stress-Strain Data for 0%

Figure 7.2 shows the normalized stress-strain curve for 1% fibers. The stress reaches an initial peak before it plateaus, which is very different from the behavior with 0% fibers. This plateau is caused by the addition of fibers in the UHPC that bridge the crack and support load after the cementitious matrix has cracked, as shown in Figure 7.3. This effect becomes even more prominent as the fiber content is increased.
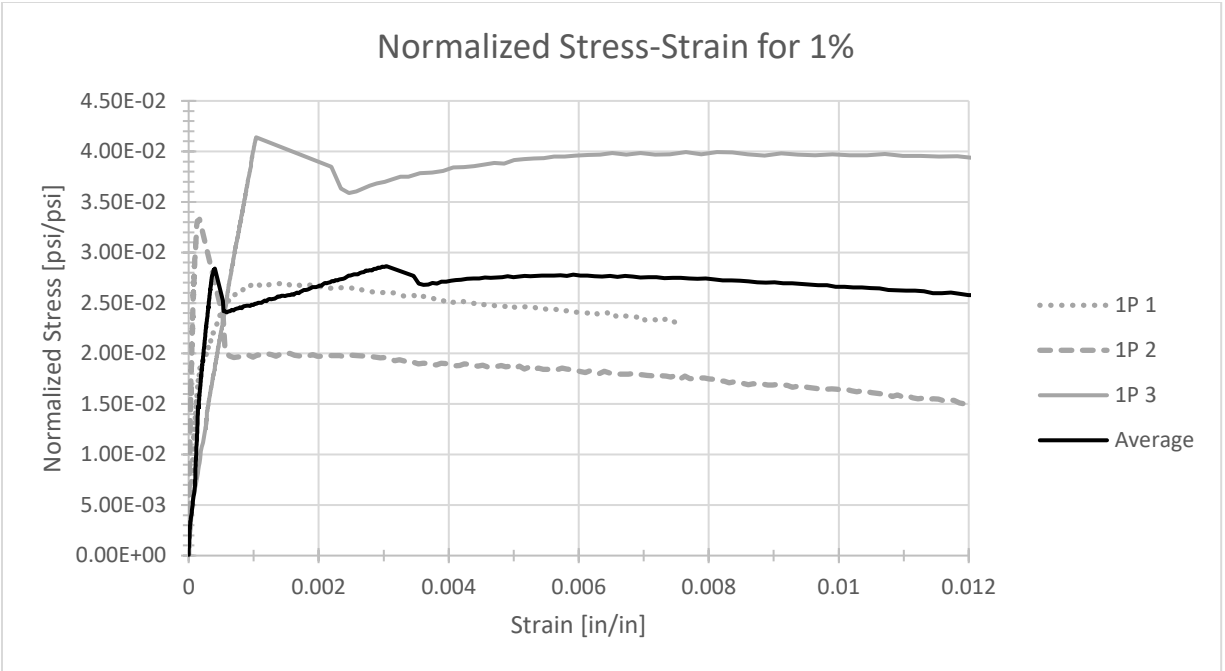
Figure 7.2 Normalized Stress-Strain Data for 1%

| (a) | (b) | (c) |

Figure 7.3 (a) Initial Crack Location, (b) Fibers Bridging Crack, (c) Post Crack

The normalized stress-strain curve for 2% fiber content shown in Figure 7.4 is similar to the overall shape of Figure 7.2. There is a little more variation as the load is continuously applied. This fluttering in the plot could have been caused again by slipping of the aluminum end anchorages.
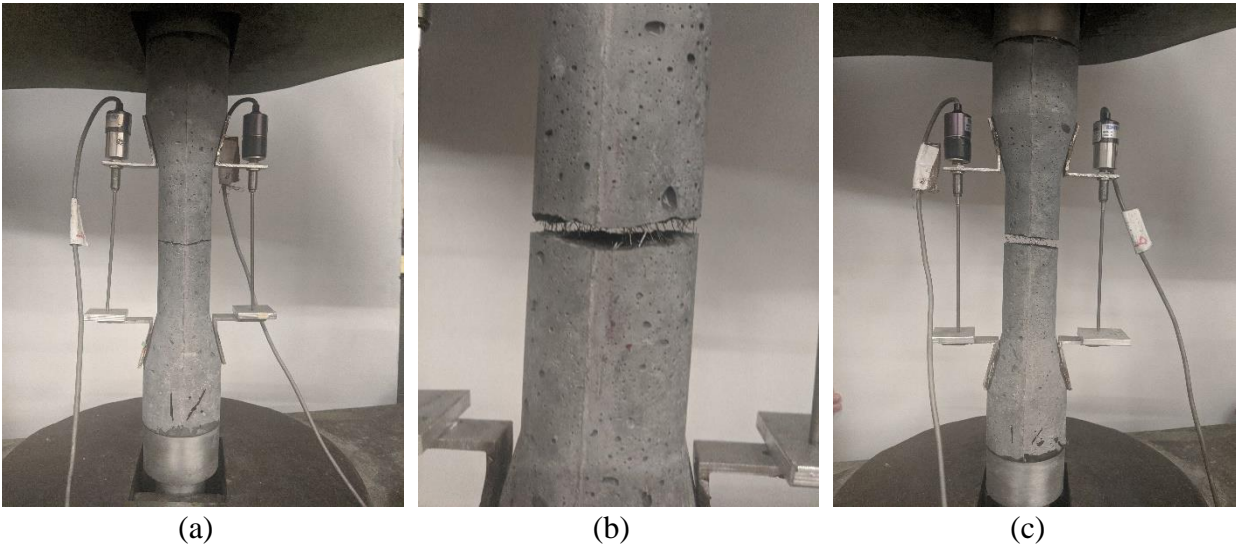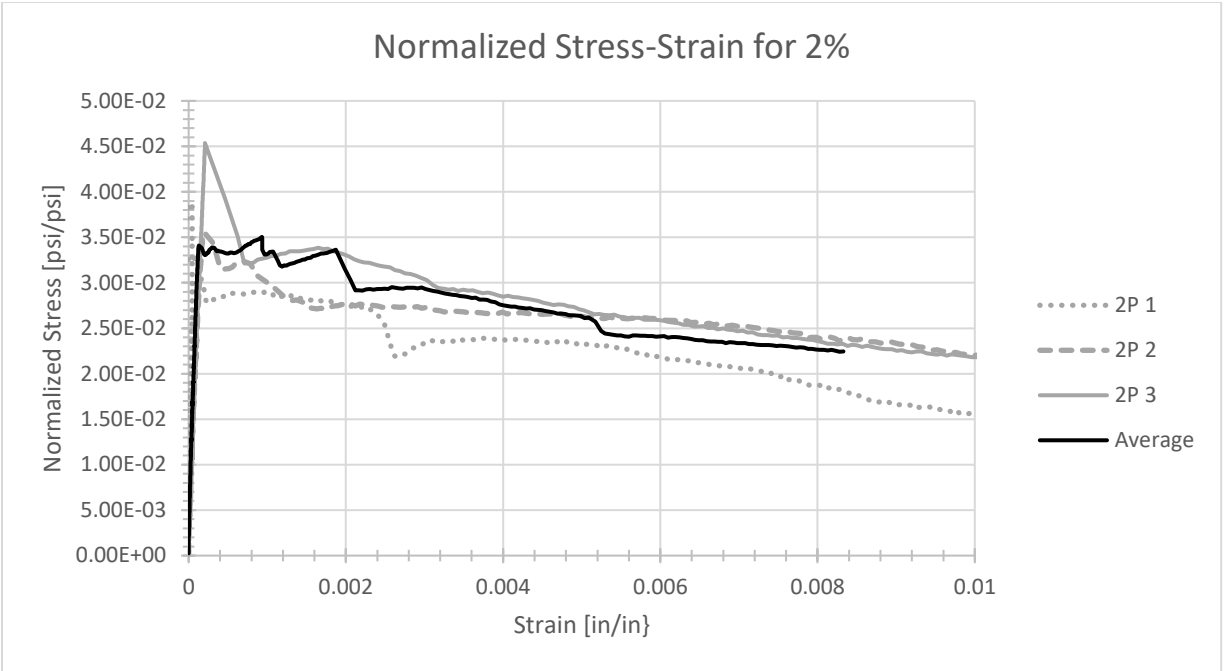
Figure 7.4 Normalized Stress-Strain Data for 2%

Figures 7.5 and 7.6 show the normalized stress-strain graphs for 4% and 6% fiber contents.

Both graphs show very similar overall shapes, with both plateauing until failure, indicating the

bridging of fibers. One of the key differences between the two fiber percentages is that at 4%

fibers content, on average, the curves are higher than that of the 6% fiber content.

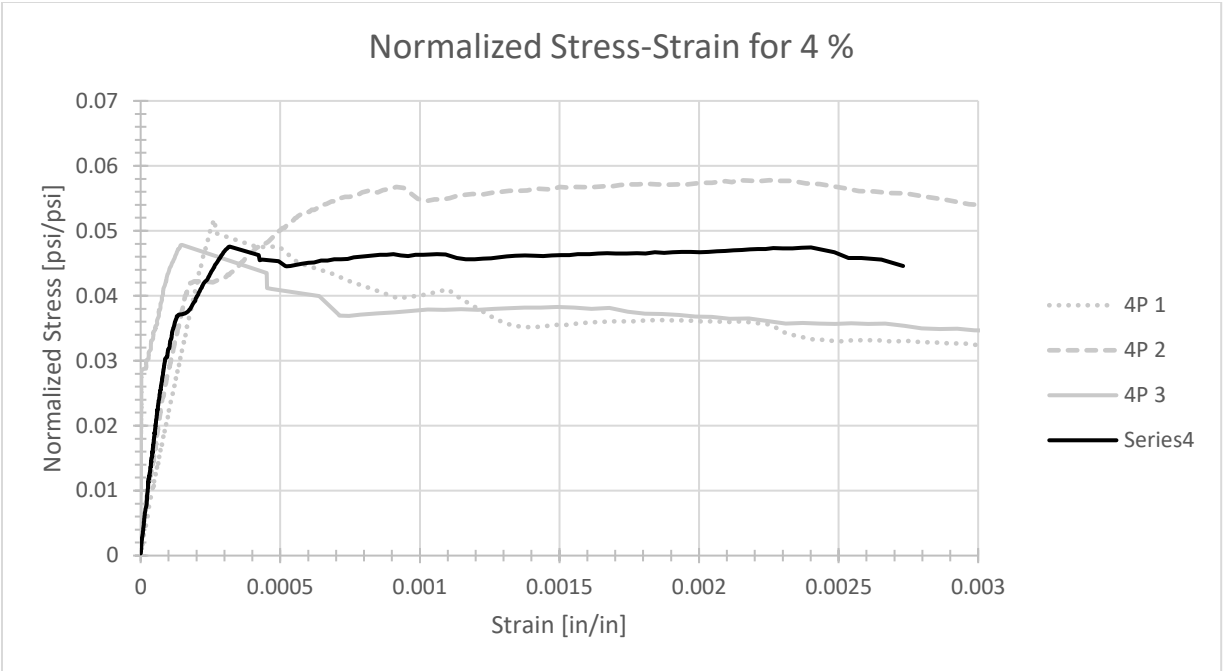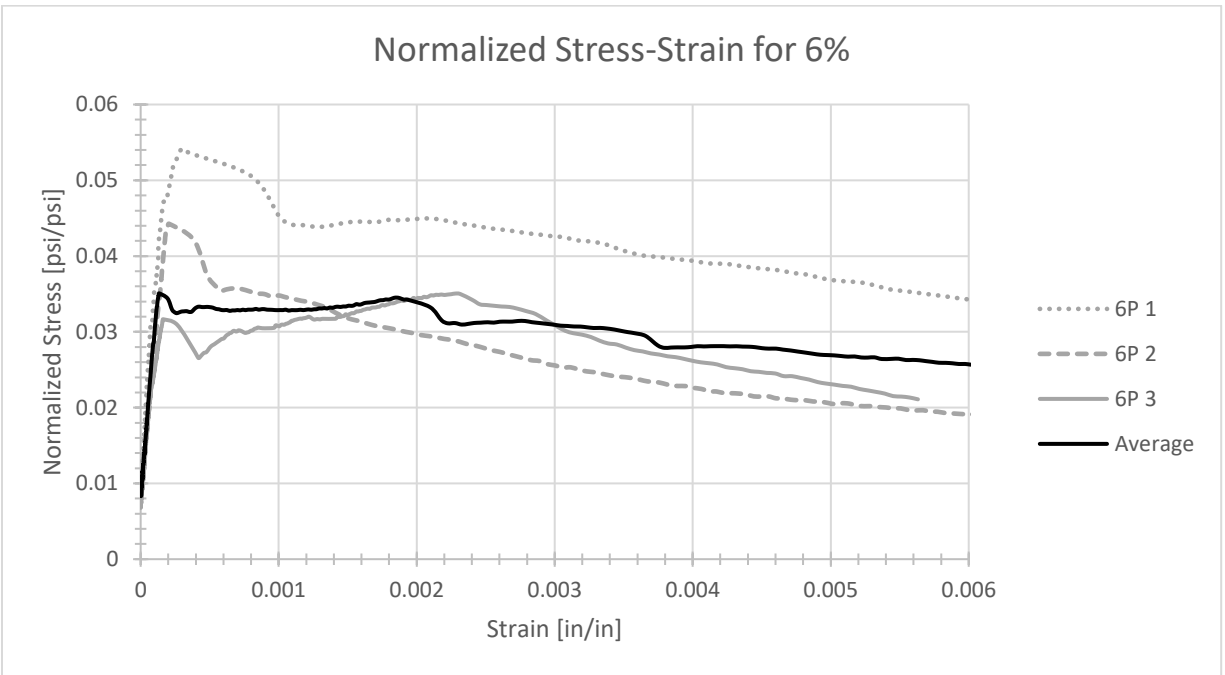*Figure 7.5 Normalized Stress-Strain Data for 4%*

Figure 7.6 Normalized Stress-Strain Data for 6%

The average of each fiber content was plotted under a single graph, which is shown in Figure 7.7. Again, it is clear to see that the 4% fiber content had the best overall behavior compared to the other fiber contents.
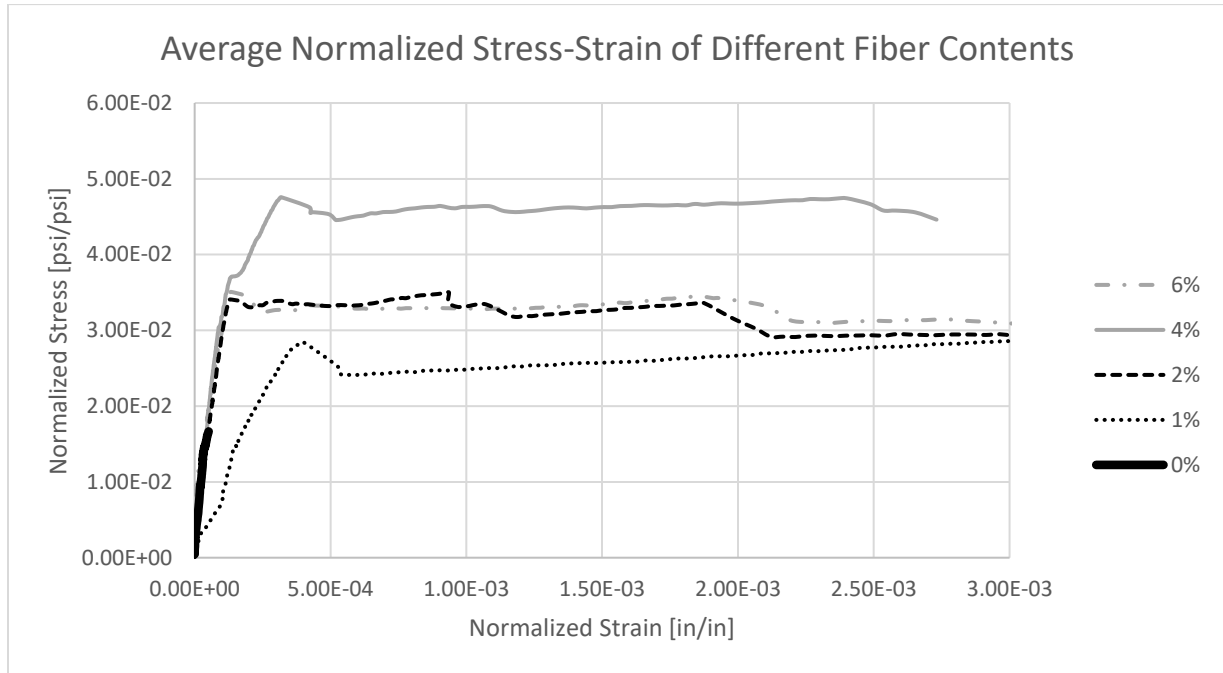
Figure 7.7 Average Normalized Stress-Strain of Different Fiber Contents

To get a better understanding of the comparisons between the fiber contents, a summary of the pre-crack modulus of elasticity and average peak pre-crack stress and strain are shown in Tables 7.1 and 7.2, respectively. Table 7.1 shows that as the fiber percentages increase, so too does the compressive strength, with the exception of 4% fiber content. The modulus of elasticity was more random than what was expected, and this could have been because of some eccentricities during the initial pulling of the specimen. The ideal modulus of elasticity is around 5,000,000 psi, with three of the specimens almost achieving that value. The modulus of elasticity was calculated by finding the slope of the initial stress-strain curve.

Table 7.1 Summary of Average Modulus of Elasticity

Fiber Percentage [%]	Average Compressive Strength [psi]	Average Modulus of Elasticity [psi]
0	16,820	5,450,000
1	17,100	1,310,000
2	18,880	4,960,00
4	18,350	2,730,00
6	20,070	4,750,00

Table 7.2 is a summary of the pre-crack behavior. The values include the average initial peak stress and strain of each fiber percentage. As shown, there is a general increasing trend with the average initial peak stress, with the exception of the 6% fiber content. This decrease in the average initial peak stress for 6% fiber content was due to a lack of uniform fiber dispersion, thus there was not enough of the concrete matrix bonding with the fibers.

Table 7.2 Summary of Average Initial Crack Behavior

Fiber Percentage [%]	Average Initial Stress [psi]	Average Initial Strain [in/in]
0	280	5.16E-05
1	495	4.02E-04
2	642	1.30E-04
4	873	3.18E-04
6	703	1.15E-04

Figure 7.8 shows one of the 6% fiber content specimens and how the fibers were oriented within the failed portion of the specimen. Due to the large percentage of fibers, it is clear to see that the fibers clustered together in certain locations, resulting in little to no concrete in between. In addition to this and the high density, many of the fibers were parallel to the failure surface, which not only lowered the initial capacity but also lowered the ability of the fibers to bridge the crack. Both of these factors caused premature fiber pull-out to occur, ultimately lowering the stress capacity of the 6% fiber content.

Figure 7.8 Example of Excessive Fiber Concentration

7.3 Post-Cracking Behavior

The graphs for the 4% and 6% data show almost identical curves to the ideal stress-strain curve. Comparing the graphs of Figures 7.5 and 7.6 to Figure 7.9, the different phases can be seen. After the initial crack, there was a plateau which lead to the ultimate stress. This fiber-bridging strength occurs when the fibers cannot continue to bridge the crack and the specimen fails.
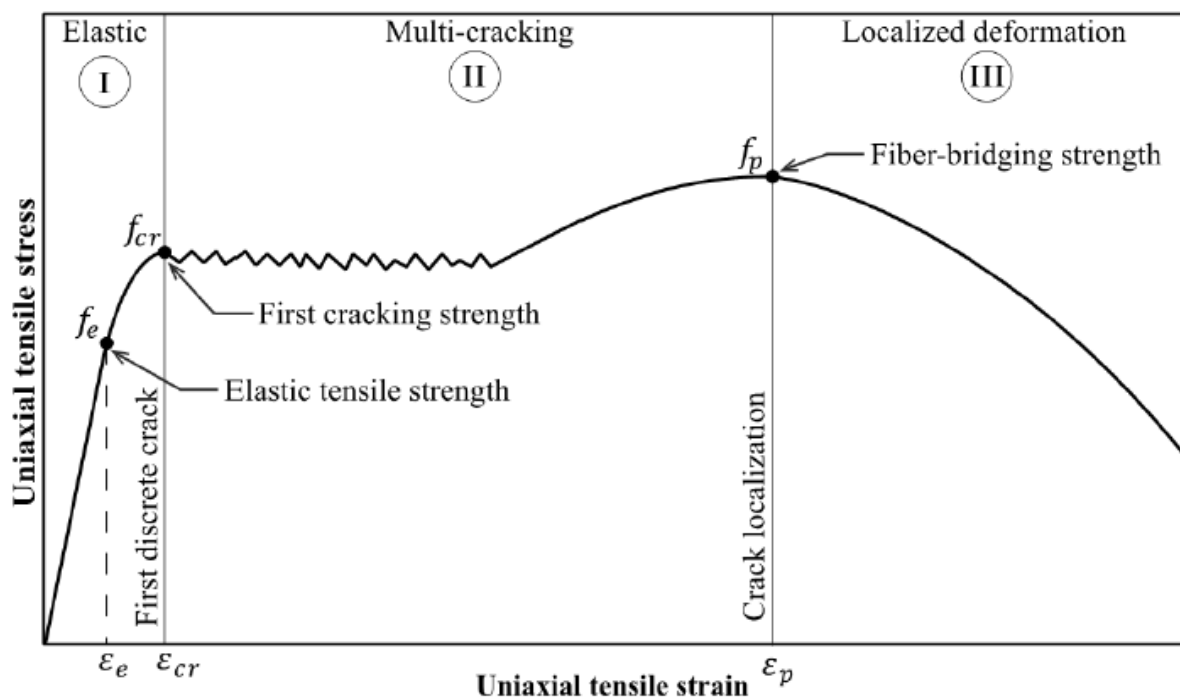

Figure 7.9 Idealized Stress-Strain Curve for UHPC (Graybeal et al., 2019)

Table 7.3 indicates the key differences between all fiber percentages, including the percentage differences between the different fiber contents. The biggest increase is from 0% to 1% fibers. The main difference between these two was just the addition of steel fibers to the mix. The highest average stress is seen with the 4% fiber content, which was measured at 870 psi or a 32% increase from the 2% fiber content. As mentioned before, the 6% fiber content, which had

the highest compressive strength, actually had a lower average peak tension stress compared to the 4% fiber content, or a 20% decrease. This was maily due to there being too many fibers disrupting the concrete matrix and premature fiber pull-out occuring.

Table 7.3 Summary of Post Crack Behavior

Fiber Percentage [%]	Average Normalized Stress	Average Ultimate Stress [psi]	Average Ultimate Strain [in/in]	% increase in Stress from Previous
0	0.0167	280	5.16E-05	0%
1	0.029	498	3.04E-03	78%
2	0.035	661	9.31E-04	33%
4	0.0474	870	2.40E-03	32%
6	0.034	699	2.87E-03	-20%

It is important to note that the plateau region happens when the fibers are bridging the intial crack, thus forming mulitple cracks. Figure 7.10 shows a graphical representation of the the post-cracking tensile strength. This reiterates that the 4% fiber content had the best tensile strength of the various fiber contents.
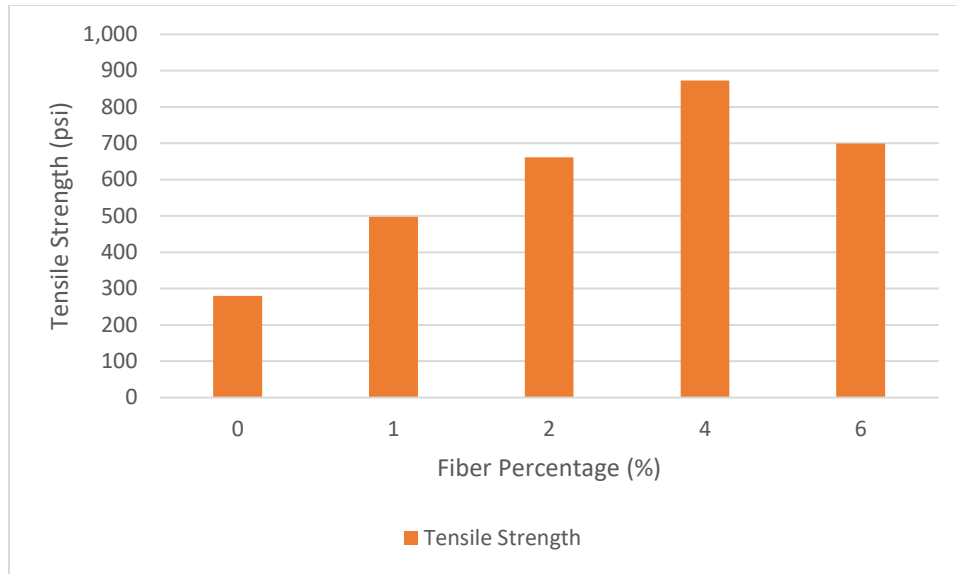
Figure 7.10 Post-Cracking Tensile Strength

The difference between the stress at the initial crack and the peak stress is shown in Table 7.4. The 0% fiber content did not plateau or have an increase because there were no fibers in the mix. Both the 1% and 2% fiber contents slightly increased indicating strain hardening; however, the behavior of the 4% fiber content showed the best behavior. Even though it did not increase, it still held constant at a higher stress than the rest throughout the plateau due to the fibers.

Table 7.4 Summary of the Change from Initial Crack to Failure

Fiber Percentage [%]	Initial Stress [psi]	Ultimate Stress [psi]	% increase after crack [%]
0	280	280	0
1	495	498	0.15
2	642	661	2.87
4	873	870	-0.34
6	702	699	-0.43

These increases indicate that the post-cracking behavior generally increases with the addition of the fibers.

7.4 Stress Distribution Behavior

7.4.1   Cylindrical Dogbone Specimen

Figures 7.11 and 7.12 show the strain data at the center and near the taper, respectively, for the first cylindrical dogbone. The first important behavior to notice is the consistency between the shape of the strain plot for each location – North, South, East, and West. Although there are slight differences, the plots are almost identical, indicating a consistent set of strains along the specimen, even adjacent to the change in cross section at the taper. As a result, the tapered shape of the dogbone reduces the potential for stress concentrations that would negatively impact the test results. Furthermore, the absolute strain values are very consistent between the strain gages at the center and near the taper.

By examining these graphs further, it is clear that the West strain was the highest, while the East strain was the lowest, sometimes dipping into the negative region. These negative strains indicate regions of compression, and along with the higher West strain pairing, it indicates imperfect alignment within the Baldwin. It is important to notice that the relative change between each quadrant – North, East, South, West – remained relatively constant. Even though there was some bending, looking at Figures 7.11 and 7.12, the change in strain occurred in a uniform fashion. This indicates that throughout the cross-section of the specimen, the strain is changing at a constant rate.
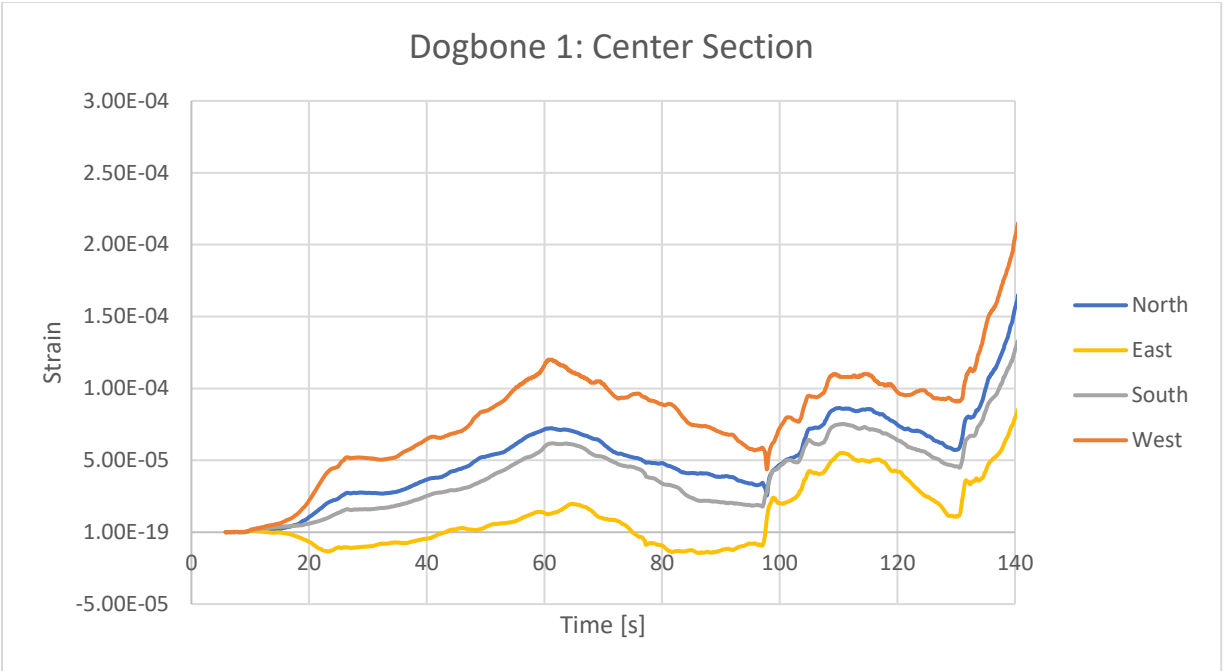
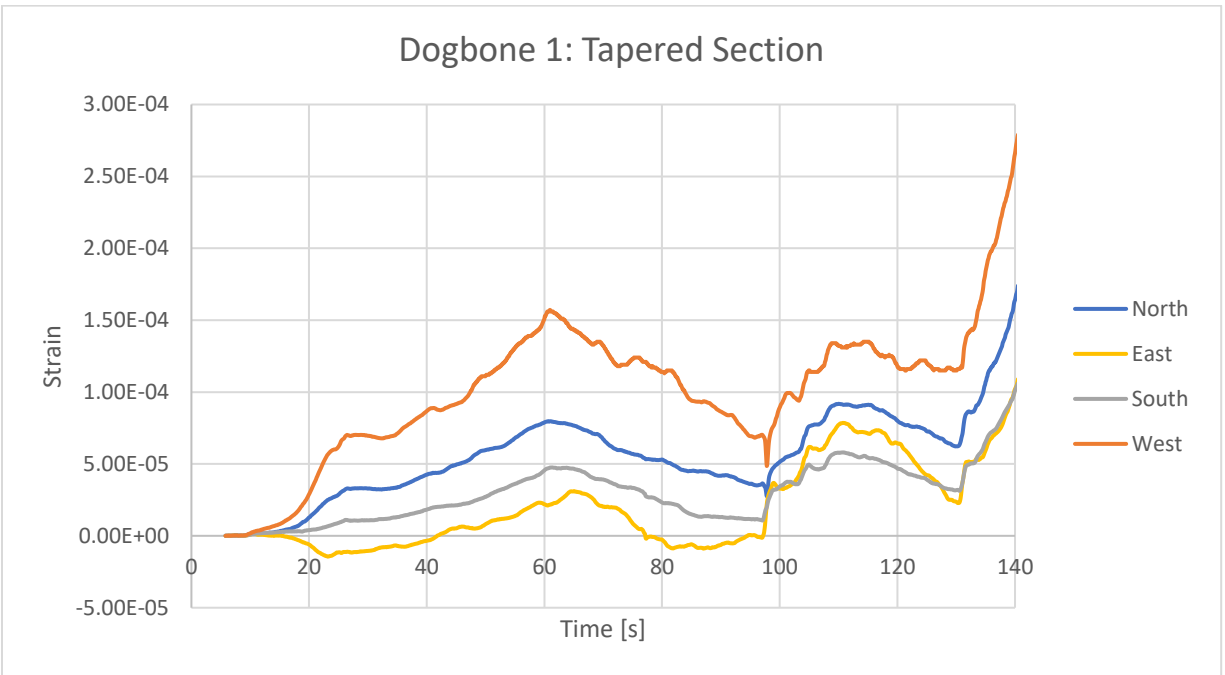*Figure 7.11 Strain Gauge data for Dogbone 1 at Center*

Figure 7.12 Strain Gauge data for Dogbone 1 at Tapered Section

Similarly, in Figures 7.13 and 7.14, the West strain was much higher than any other side, most notably the East side, which experienced a negative strain again. This indicates bending on the specimen, which was most likely caused by an eccentricity. It is clear that the strains are changing at a similar rate, which further solidifies that the stress distribution in the cylindrical dogbone are uniform. However, although the plots are again very similar between the center and near the taper, the absolute values are different between the two locations.
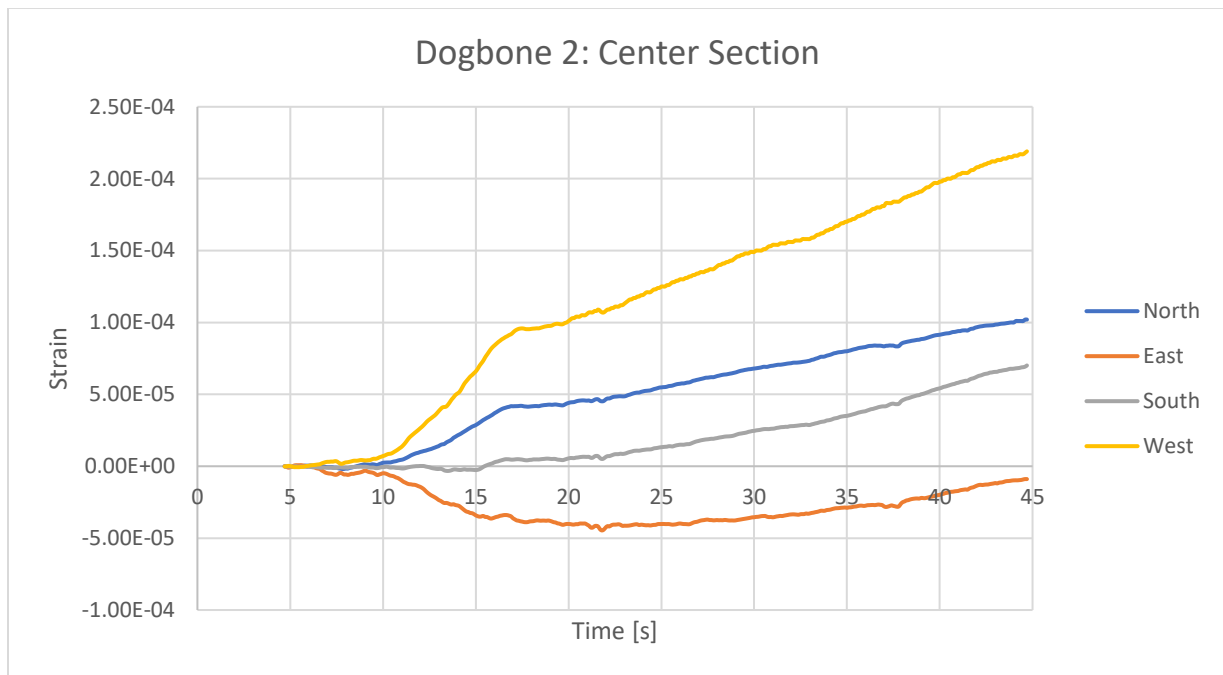

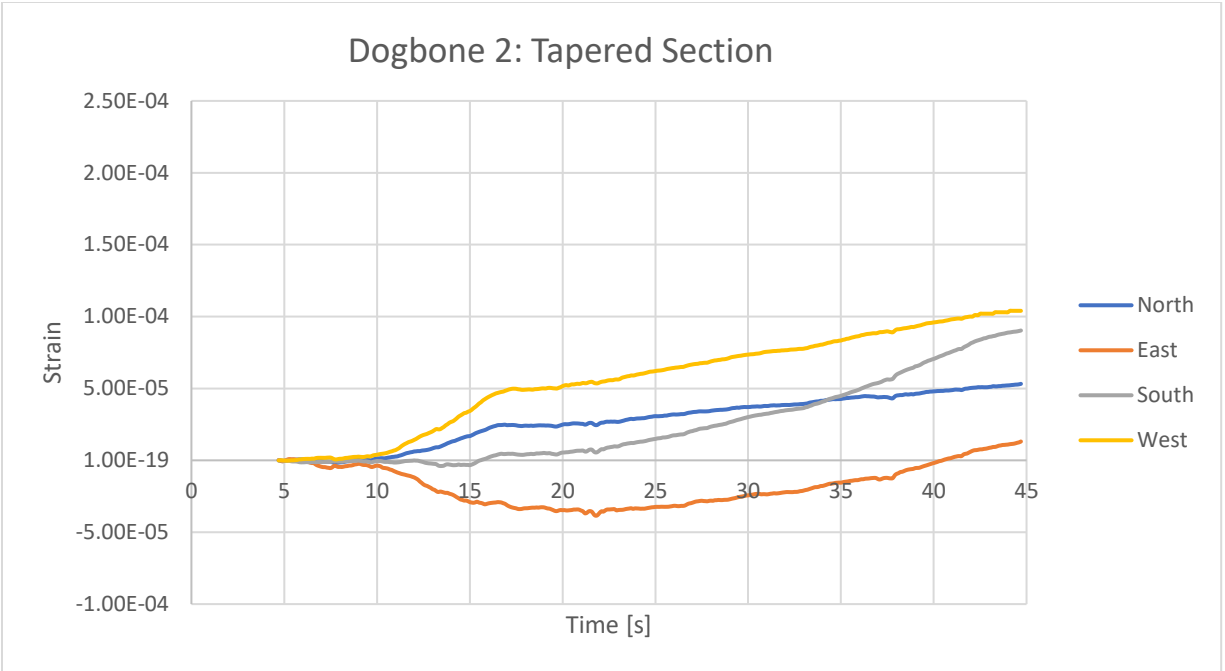*Figure 7.13 Strain Gauge data for Dogbone 2 at Center*

Figure 7.14 Strain Gauge data for Dogbone 2 at Tapered Section

Figure 7.15 shows the difference between the strain at the center and near the taper for the

first cylindrical dogbone, while Figure 7.16 shows the difference between the strain at the center

and near the taper for the second cylindrical dogbone specimen. The maximum strain of each

quadrant and section were found and then compared to one another. Figure 7.15 shows that the

maximum difference between the tapered section and the center was approximately 30% on the
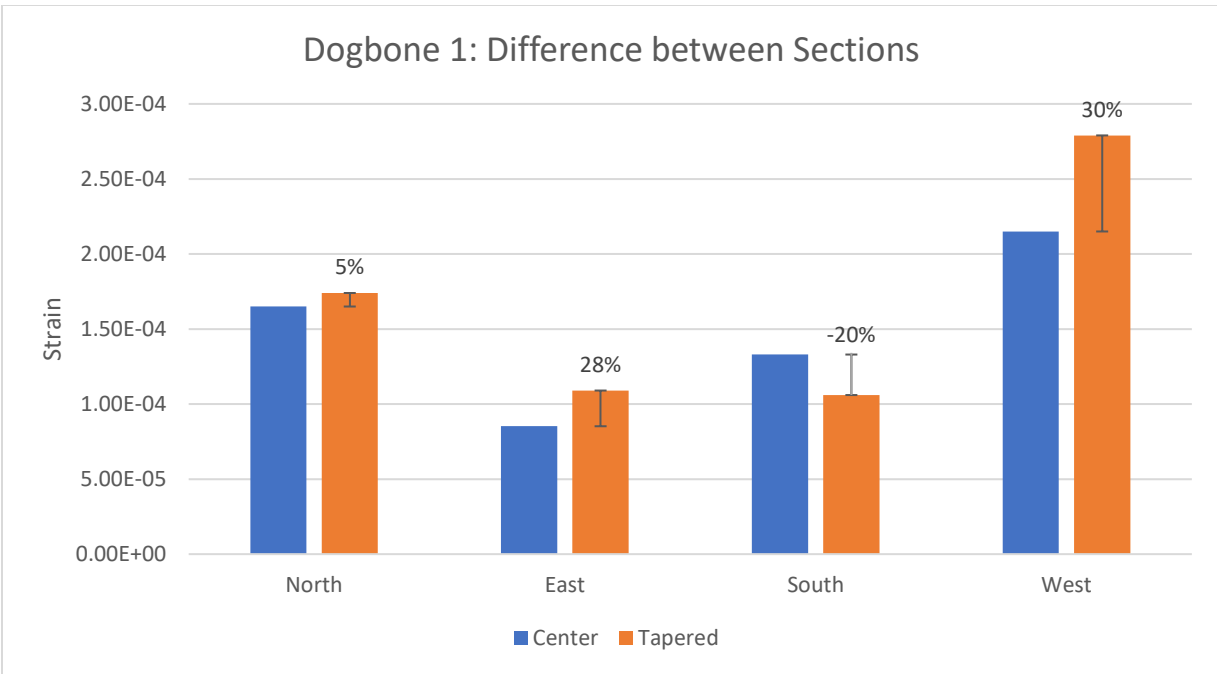
West side.

Figure 7.15 Difference between Strain at Center vs. at Tapered Section for Dogbone 1

For the second cylindrical dogbone, the differences are much larger. However, unlike in Figure 7.15 where all the maximum strain was positive, in Figure 7.16 it is clear that the East strain is negative, for both the center and the tapered section. This is one of the reasons that the differences are much larger, as the eccentricity exaggerates the data.
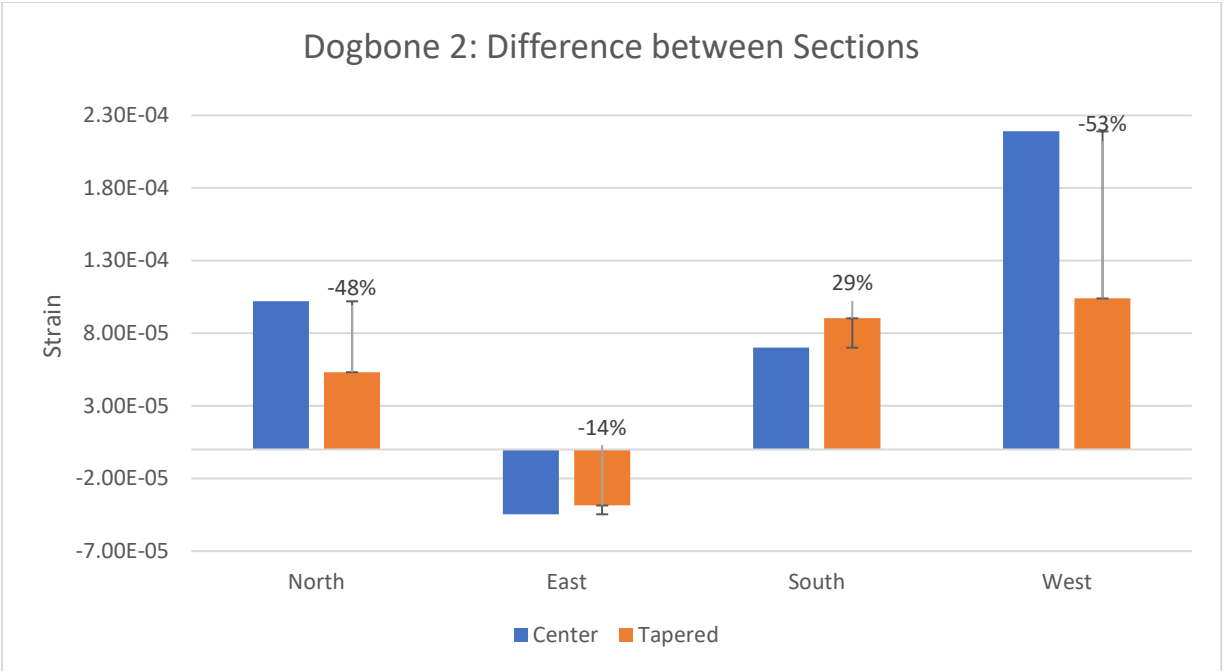
Figure 7.16 Difference between Strain at Center vs. at Tapered Section for Dogbone 2

The average percentage difference between the center and the tapered section was calculated from both cylindrical dogbones and is shown in Table 7.5. The East and South directions have the lowest percent difference, whereas North and West have the greatest. This again indicates imperfect alignment of the specimen within the Baldwin. The closer the percentage difference is to zero, the more uniform the stress distribution is between the center and the tapered section.

Table 7.5 Percentage Difference between Tapered Section and Middle Section

	Percentage Difference [%]
North	27
East	25
South	25
West	41

64

The idealized ANSYS model for the cylindrical dogbone specimen is shown in Figure 7.17. The figure shows the cross-section of the center, and it is clear that throughout the cross-section, the stress is very evenly distributed. As expected, at the tapered section there was an increase in the stress. From the data collected, the percentage difference between the tapered section and the middle section, if no bending was involved, is only 20%.
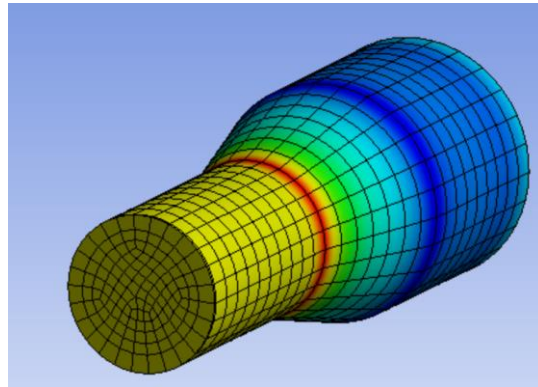

Figure 7.17 ANSYS Model of a Cross-Section of the Cylindrical Dogbone

The uniform distribution of stress throughout the cross-section was expected because of how the stress is distributed in a typical cylinder, which is further discussed in Section 7.4.2.

7.4.2 Cylindrical Specimen

Figure 7.18 shows the strain distribution of the first cylinder. Again, bending can be seen here. The West and South directions have an almost identical rate of change and strain readings, whilst the North direction has a slightly higher strain. The strains of the second cylinder, shown in Figure 7.19, follow a similar pattern. Although the strains are not identical, the rate at which they change are very similar throughout each direction, indicating uniform stress distribution.
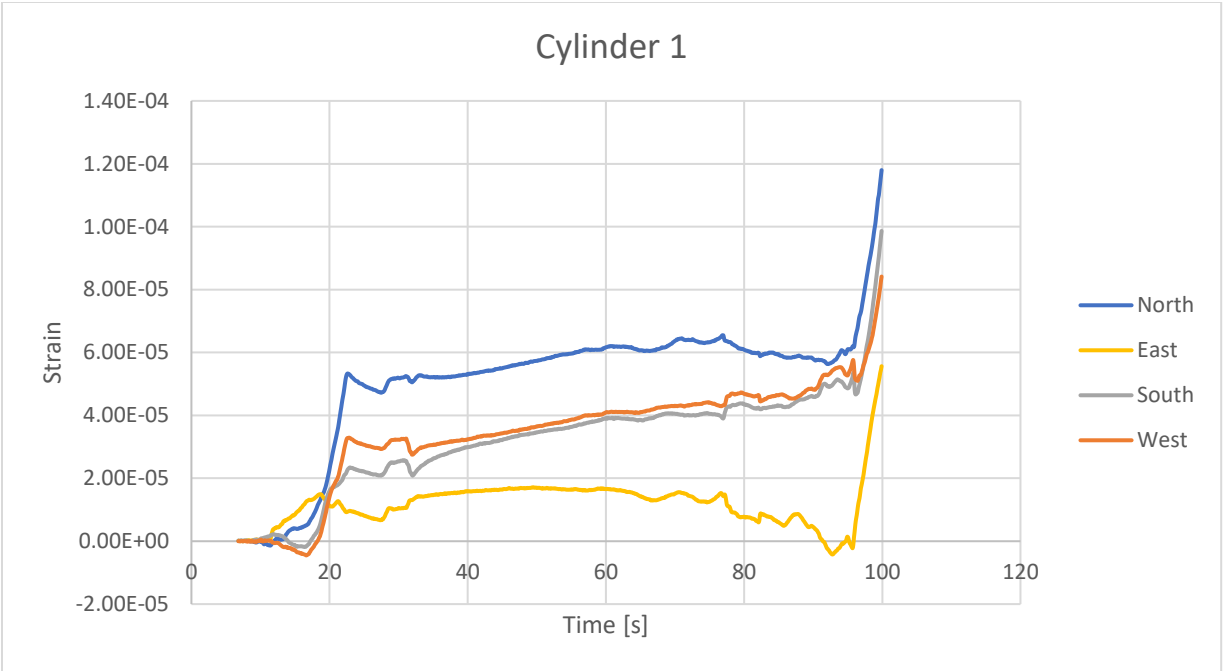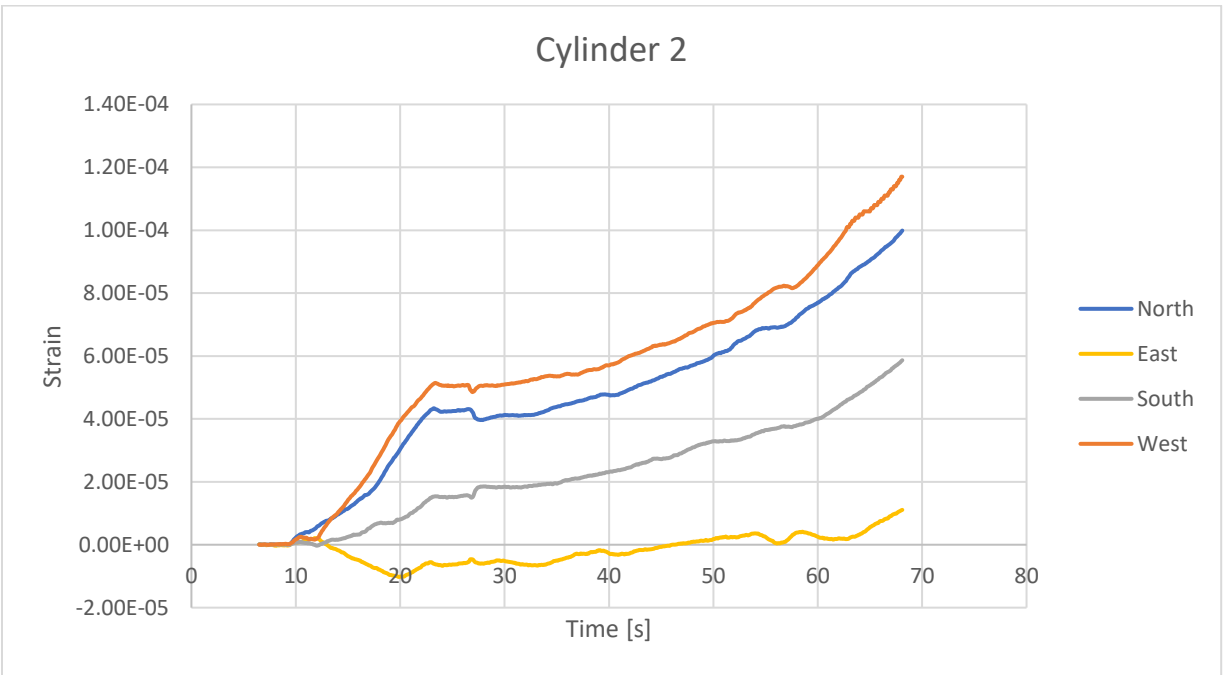
Figure 7.18 Strain Gauge data for Cylinder 1

Figure 7.19 Strain Gauge data for Cylinder 2

The ANSYS model of the cylinder also indicates that the strain is uniformly distributed throughout the cross-section as shown in Figure 7.20. There is a peak in strain at the ends, however this was due to the fixed support constraints from the software and does indicate the confining effect of the end attachments and potential stress concentrations for this specimen type.
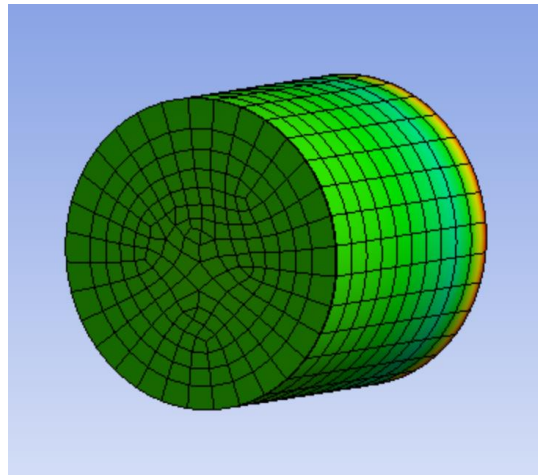

Figure 7.20 ANSYS Model of a Cross-Section of the Cylinder

This idealized uniform distribution, which is similar to the cylindrical dogbone, thus validating that the cylindrical dogbone specimen can be used as the DTT specimen.

7.4.3   FHWA Specimen

The strain distribution for the first FHWA specimen is shown Figures 7.21 and 7.22. Once again, the West strain is much higher than the rest, while the East strain was negative at both the center and the corner. This behavior indicates there was an eccentricity during the test. In Figure 7.22, the North and South corner strains significantly changed when compared to the North and South center strains shown in Figure 7.21. This indicates that the stress distribution from the center of the specimen to the corner is not uniform, which leads to stress concentrations and potentially erroneous results.
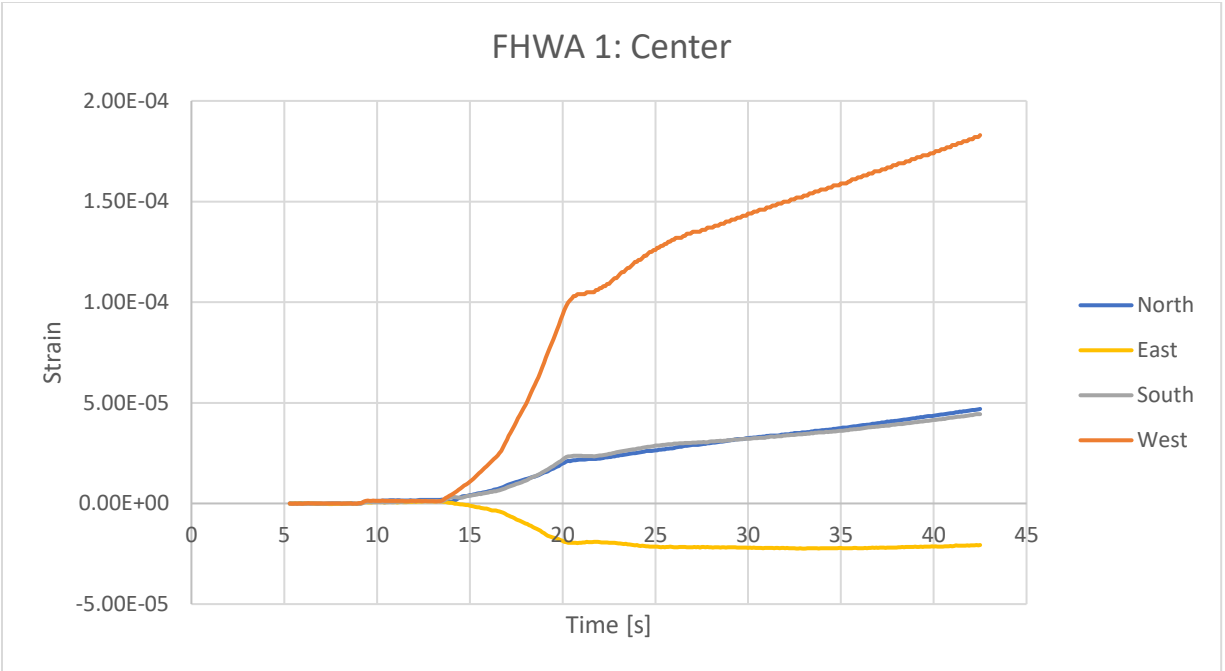
Figure 7.21 Strain Gauge data for FHWA 1 at Center
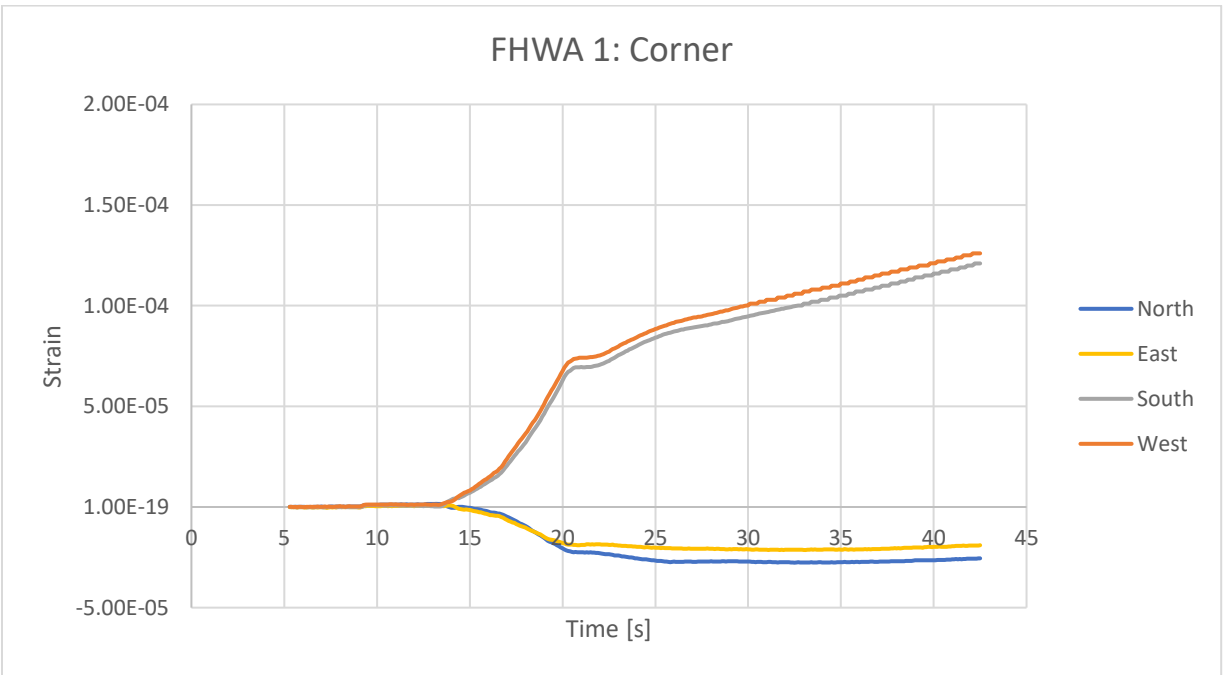

Figure 7.22 Strain Gauge data for FHWA 1 at Corner

A similar trend was observed in the second FHWA specimen. In both Figure 7.23 and 7.24, the West strain was the highest. Both the East and South strain at the corner increased compared to the center, while the North strain at the corner decreased, indicating bending.
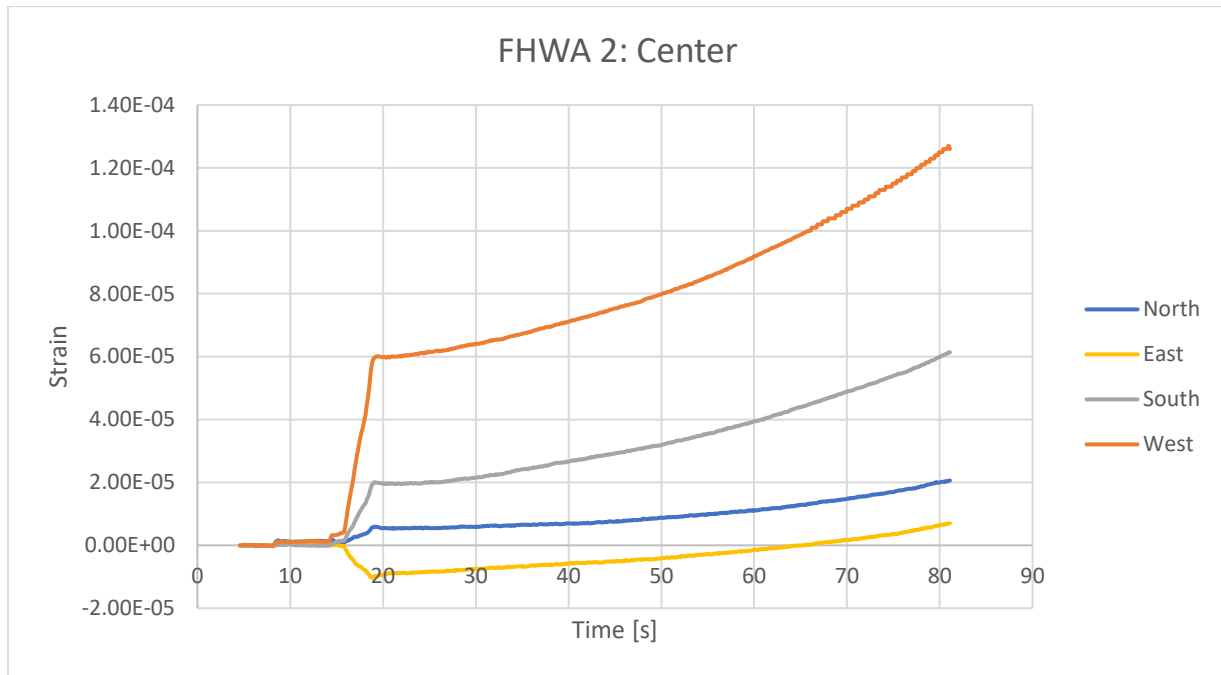
Figure 7.23 Strain Gauge data for FHWA 2 at Center
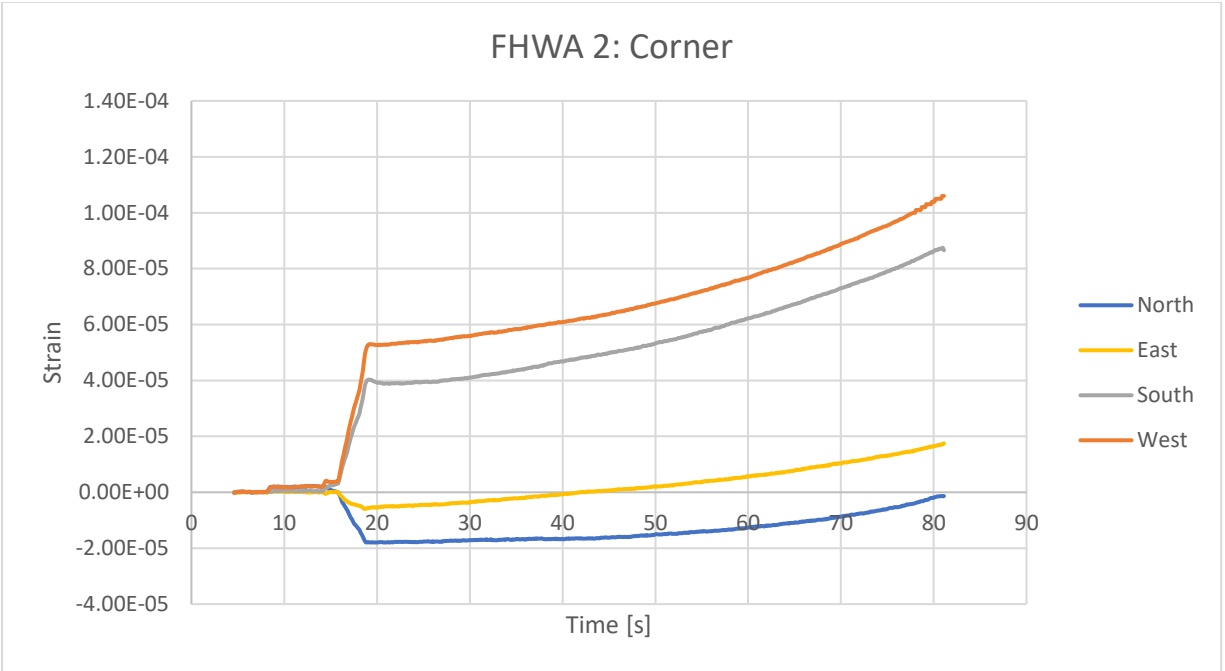
Figure 7.24 Strain Gauge data for FHWA 2 at Corner

Figure 7.25 and 7.26 show the difference between the maximum strains for the two FHWA

specimens. The differences between the center strains and the corner strains in Figure 7.25 have

a wide range. The largest difference, of 173%, was seen on the South face, while the smallest

difference was observed on the East face, at 5%. This trend continued in Figure 7.26, with the

largest difference at 270% on the East face, while the smallest difference was on the West face at

17%.

Figure 7.25 Difference between Center and Corner on FHWA 1

Figure 7.26 Difference between Center and Corner on FHWA 2

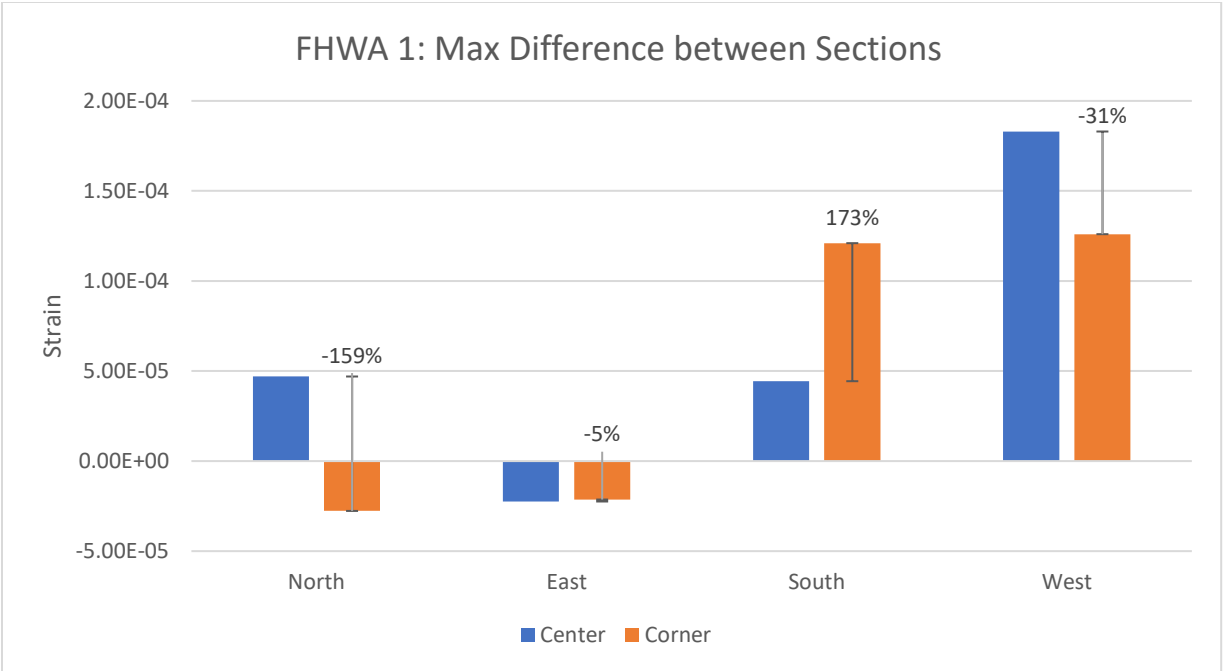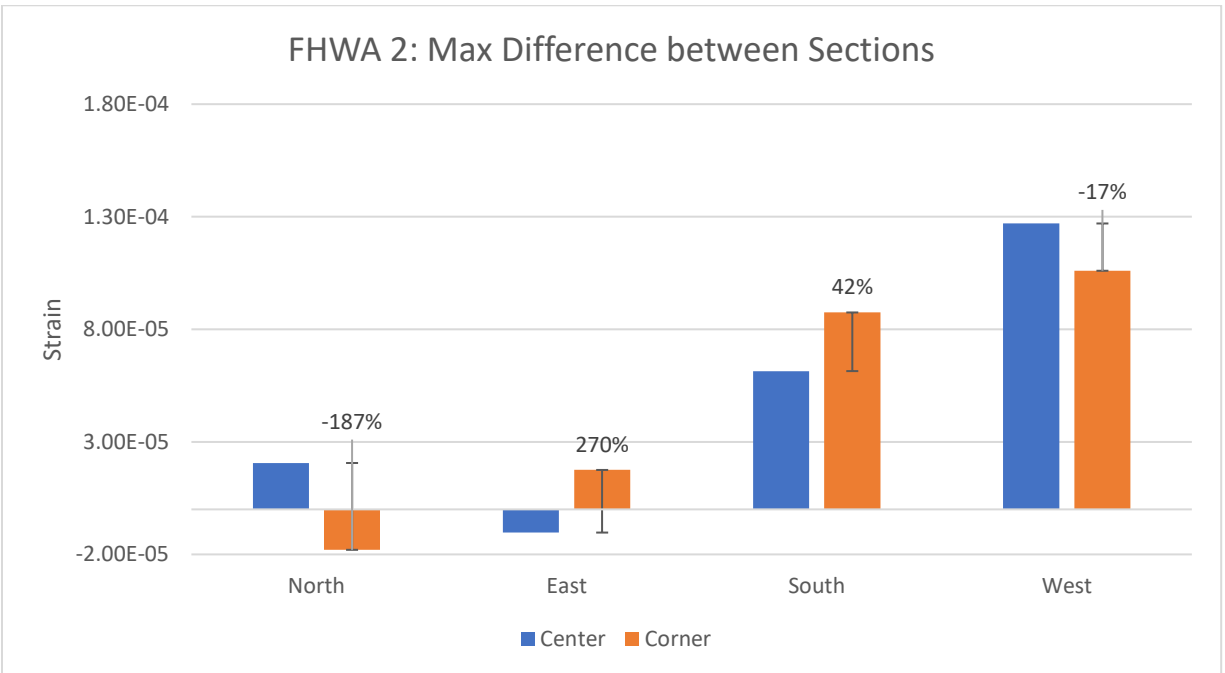The ANSYS model shown in Figure 7.27 paints a very similar picture. At the corners there is a concentration of stresses, and as the stress moves towards the center, it changes significantly.

According to the data that was collected, the percentage difference between the corners and the center changed at different locations throughout the specimen. On average, the percentage difference was calculated at 88%.
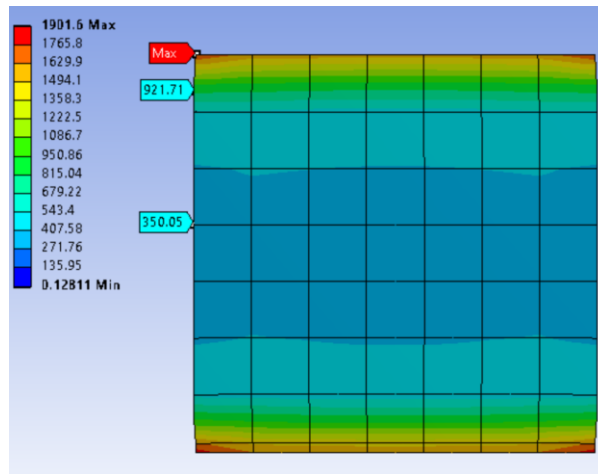
Figure 7.27 ANSYS Model of the FHWA Specimen

Even though this was an idealized model, with no eccentricities applied, there were still large differences not only between the corner and the center but also throughout the thickness of the specimen. These large differences could provide inaccurate and inconsistent data, which verifies the need for a specimen to have reduced stress concentrations and improved stress distributions, such as the cylindrical dogbone specimen.

8 Findings, Conclusion, and Recommendations

This chapter summarizes the findings, conclusions, and recommendations from this research study.

8.1 Findings

Through the analysis of the DTT on the cylindrical dogbone specimen, certain key findings were determined. The main reason for the DTT on UHPC was to determine where the optimum fiber content for strain hardening would occur. The highest overall ultimate tensile strength was found at a 4% fiber content. The post-cracking behavior and the ultimate tensile strength of the 6% fiber content specimen was similar to that of the 2% fiber content specimen, showing that the 'tipping' point of the fiber content is around the 4% fiber content. The pre-cracking tensile strength of the 4% fiber content was also the highest of any fiber content.

Once the first crack formed, a plateau effect can be observed in the stress-strain graph. This plateau is caused by the fibers bridging the crack while the specimen continues to crack at other locations, forming multiple cracks within the specimen. This leads to the ultimate stress, where the fibers cannot bridge the gap any longer and the specimen fails. This plateau started at 1% fiber content, which indicates that to achieve the best performance of UHPC, adding fibers will definitely improve the post-cracking performance.

One of the concerns with using a cylindrical dogbone specimen was that the crack would not occur in the center section, which was the desired location. However, throughout testing of the UHPC dogbone specimens with fibers, the crack propagated from the center. Along with this, there were no bond failures between the aluminum ends and the cylindrical dogbone, indicating excellent potential as an accurate and repeatable test method.

Stress distribution studies of the different tension test specimen types also indicated that the cylindrical dogbone specimen provided the greatest potential for accurate and repeatable results. The enlarged ends of the cylindrical dogbone specimen also overcame the limitation of potential bond failures to the end anchorages that occur with a straight cylindrical specimen. As for the FHWA Specimen, during testing and from the analytical model, it was clear that the specimen had issues with squeezing of the ends. This caused high stresses where the end anchorages met the middle section of the specimen, thus allowed for premature failure.

8.2 Conclusions

In conclusion, the cylindrical dogbone provided the best overall specimen for a DTT. As the stress distribution study showed, the stress differences between the tapered section and the middle section were much smaller than that of the FHWA specimen, indicating that it would produce more reliable and consistent results. From the ANSYS model, the cylinder had a uniform stress distribution, which would make it the best specimen, however the small surface area at the ends caused issues with bond failures at the end anchorages. The cylindrical dogbone has a 3 inch diameter at the ends, which provides an adequate area for the epoxy to adhere to, rather than the 2 inch diameter of the cylinder. This increase also meant that the JB ClearWeld adhesive was more than adequate for the DTT.

The DTT showed that the biggest increase in the tensile strength of UHPC occurred at a 4% fiber content. Increasing to 6% fiber content actually decreased the average peak tensile capacity and provided similar performance and results to the 2% fiber content specimen. The post-cracking behavior of the 4% fiber content perfectly plateaued until failure, which shows the importance of adding fibers. The main reason that the 6% fiber content did not improve the

74

tensile capacity was due to the clustering of the fibers within the specimen. This caused a break in the concrete matrix and actually lowered the ability to distribute the stress uniformly.

8.3 Recommendations

Based on the findings and conclusions, there can be some improvements for future studies:

- Improve the tapered section by making it a continuous curve rather than coming to a hard point. This will reduce the stress concentrations even more.

- Increase the number of LVDTs around the specimen. This will not only provide better feedback on whether the specimen is aligned correctly, but also provide a 360-degree view of the specimen.

- Change the aluminum end anchorages to a harder metal to avoid slipping within the test machine grips during testing.

- Perform a study examining the effects of using different fiber shapes in the cylindrical dogbone specimen.

- Perform a study examining the effects of eccentricity on the stresses within the cylindrical dogbone specimen.

9   References

Choi, S.-W., Choi, J., & Lee, S.-C. (2019). Probabilistic Analysis for Strain-Hardening Behavior of High-Performance Fiber-Reinforced Concrete. *MDPI: Materials*.

Deng, F., Ding, X., Chi, Y., Xu, L., & Wang, L. (2018). The pull-out behavior of straight and hooked-end steel fiber from hybrid fiber reinforced cementitious composite: Experimental study and analytical modelling. *Composite Structures, 206, 693-712.*

FHWA (2019). Ultra-High Performance Concrete. Retrieved from https://highways.dot.gov/bridges-and-structure/ultra-high-performance-concrete/ultra-high-performance-concrete

Graybeal, B. A., & Baby, F. (2013). Development of Direct Tension Test Method for Ultra-High-Performance Fiber-Reinforced Concrete. *ACI Materials Journal, March-April*, 117-186.

Graybeal, B. A. (2019). Design and Construction of Field-Cast UHPC Connections. *FHWA-HRT-19-011.*

Graybeal, B. A. (2018). Properties and Behavior of UHPC-Class Materials, *FHWA-HRT-18-036.*

Graybeal, B. A. (2011). Ultra-High Performance Concrete. *FHWA-HRT-11-038*

Isojeh, B., El-Zeghayar, M., & Vecchio, F. J. (2017). Fatigue Behavior of Steel Fiber Concrete in Direct Tension. *ASCE, J. Mater Civ. Eng. 29(9)* (04017130).

Kwan, A. K. H., & Chu, S. H. (17 September 2018). Direct tension behaviour of steel fibre reinforced concrete measured by a new test method. *Engineering Structures, 176*, 324-336.

Parvez, A., & Foster, S. J. (2015). Fatigue Behavior of Steel-Fiber-Reinforced Concrete Beams. *ASCE: J. Struct. Eng., 141(4)*.

Ross, B. E., & Hamilton III, H. R. T. (2010). Evaluation of strain gage lengths for testing limestone and granite aggregate concretes. *Construction and Building Materials, 25*, 406-408.

Savino, V., Lanzoni, L., Tarantino, A. M., & Viviani, M. (26 July 2018). Tensile constitutive behavior of high and ultra-high performance fibre-reinforced-concretes. *Construction and Building Materials*(186), 525-536.

Wille, K., El-Tawil, S., & Naaman, A. E. (2014). Properties of strain hardening ultra high performance fiber reinforced concrete (UHP-FRC) under direct tensile loading. *48*, 53-66.

10 Appendix

Tables

Table A 1 UHPC Fiber Composition and Compressive Strength

Component	Unit	Percentage of Fibers (%)				
		0	**1**	**2**	**4**	**6**
Silica Fumes	*lbs*	1.52	1.51	1.49	1.46	1.43
GGSFB	*lbs*	4.57	4.52	4.48	4.39	4.30
Type I Cement	*lbs*	9.14	9.05	8.96	8.77	8.59
Steel Fibers	*lbs*	0.00	1.00	2.01	4.02	6.03
Masonry Sand	*lbs*	15.23	15.08	14.93	14.62	14.32
Water	*lbs*	3.05	3.02	2.99	2.92	2.86
HRWR	*ml*	81.08*	80.27*	79.46*	99.46**	97.39**
Compressive Strength	*psi*	18543	17263	19044	18853	19753
	psi	16816	17067	19212	18036	20057
	psi	15090	17680	18062	18170	20390

* - oz./cwt of 18

** - oz./cwt of 23

Table A 2 Composition of GGBFS

Sample	SiO_2	Al_2O_3	Fe_2O_3	CaO	Na_2O	K_2O	SO_3	P_2O_5	TiO_2	LOI
GGBFS	29.96	12.25	0.52	45.45	0.31	0.38	3.62	0.04	0.46	2.39

Figures

Figure A. 1 Setup for cylindrical dogbone casting

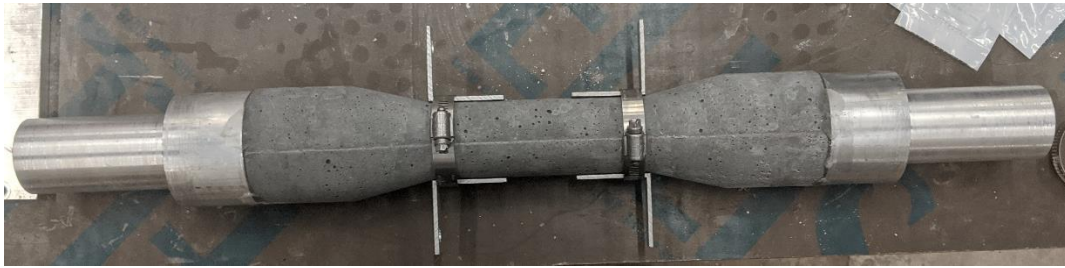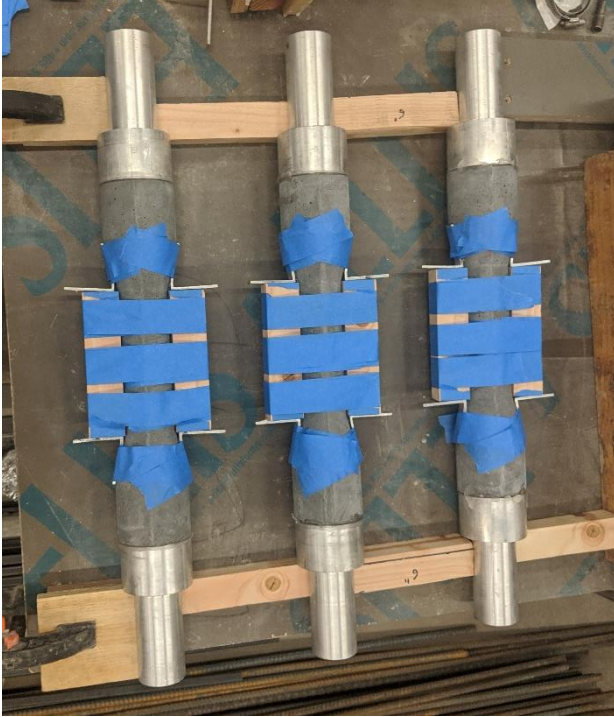*Figure A. 2 Hose-clamped LVDT Brackets*

Figure A. 3 Cylindrical Dogbone Specimen Gluing Setup

(a)   (b)

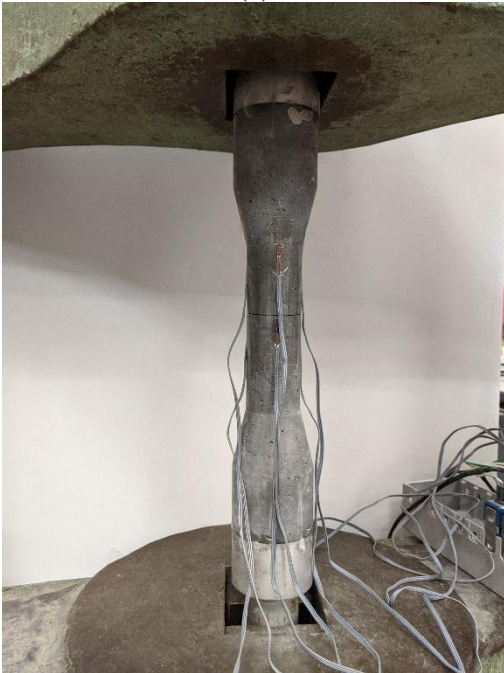*Figure A. 4 (a) Drying Setup for LVDT Brackets (b) Spacers for LVDT Brackets*
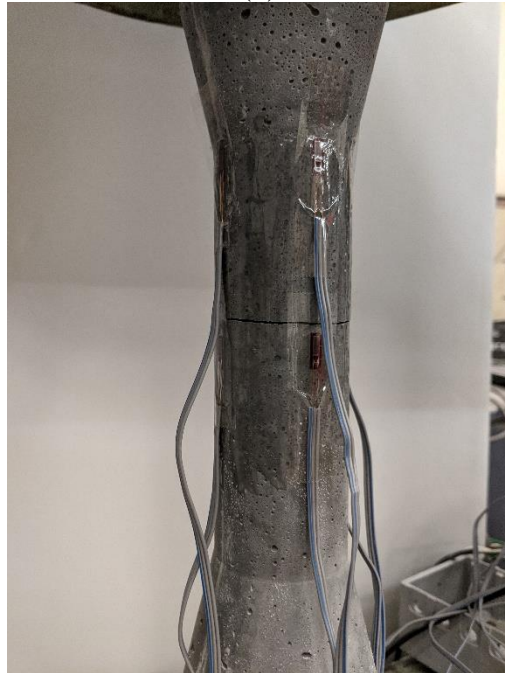

Figure A. 5 Multiple Crack Formation

(a)

(b)

(c)

(d)

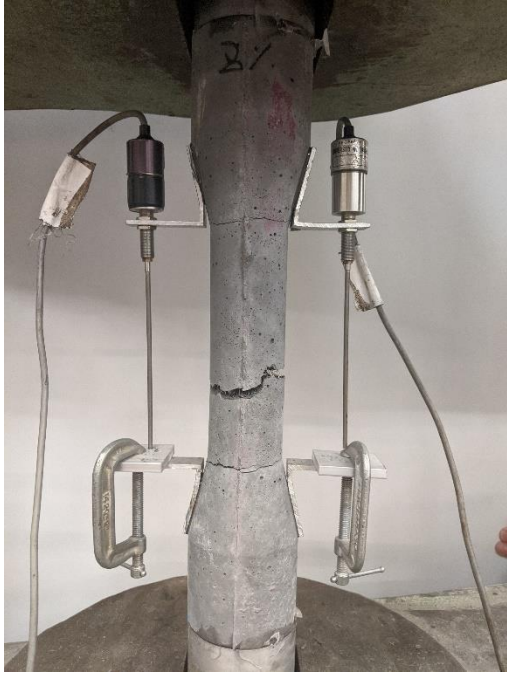*Figure A. 6 Ideal Crack Locations*

(a)

(b)

(c)

(d)

Figure A. 7 Cracks from Misalignment of Specimen

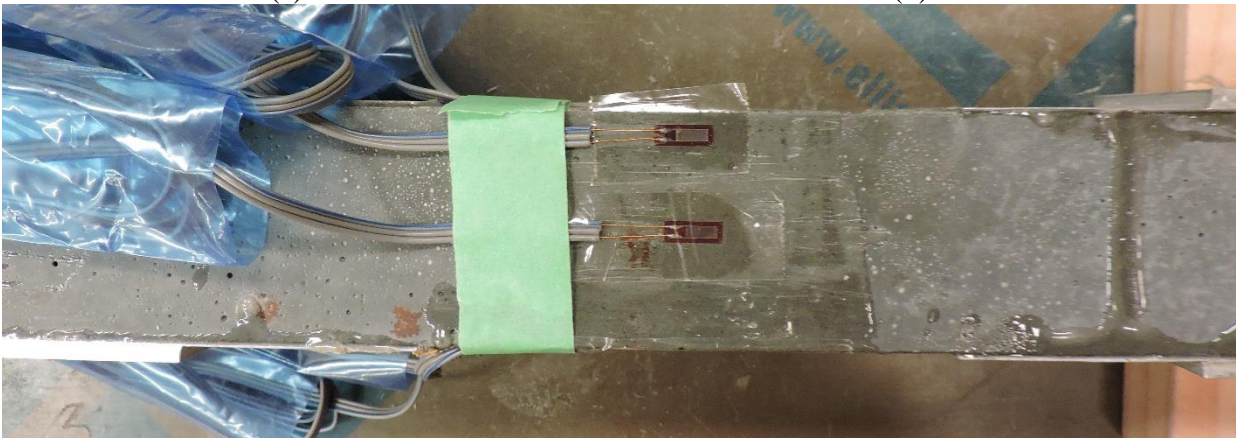(a)   (b)

Figure A. 8 (a) Cylinder Setup (b) FHWA Setup

(a)

(b)

(c)

Figure A. 9 Strain Gauge Location in (a) Cylindrical Dogbone (b) Cylinder (c) FHWA Specimen